TEMPERATURE DEPENDENCE OF THE PENETRATION DEPTH IN THE UNCONVENTIONAL SUPERCONDUCTOR Sr_2RuO_4

BY

BRIAN DAVID YANOFF

B.A., Swarthmore College, 1993
M.S., University of Illinois, 1994

THESIS

Submitted in partial fulfillment of the requirements
for the degree of Doctor of Philosophy in Physics
in the Graduate College of the
University of Illinois at Urbana-Champaign, 2000

Urbana, Illinois

TEMPERATURE DEPENDENCE OF THE PENETRATION DEPTH IN THE UNCONVENTIONAL SUPERCONDUCTOR STRONTIUM RUTHENATE

Brian David Yanoff, Ph.D.
Department of Physics
University of Illinois at Urbana-Champaign, 2000
Dale J. Van Harlingen, Advisor

We have constructed a high resolution tunnel-diode oscillator based measurement system suitable for measuring the temperature dependence of the magnetic penetration depth of superconductors, $\lambda(T)$, at very low temperatures. I report on measurements of $\lambda(T)$ in high quality single crystals of the perovskite superconductor Sr_2RuO_4 down to 0.04 K. We observe quadratic temperature dependence at low temperatures. There is no sign of the crossover or second phase transition predicted for a multi-band superconductor. We argue that power law behavior is consistent with an energy gap with nodes, and discuss how the observed quadratic dependence can arise from several possible mechanisms. We propose that non-local effects may be more important in determining the temperature dependence than impurity scattering, and are sufficient to explain the deviation from the linear behavior expected for local superconductors with line nodes. These results are inconsistent with the candidate *p*-wave states predicted by leading theories.

This thesis is dedicated to my wife, Liz. Without her love, encouragement, support, patience and understanding, this thesis would not be what it is. And I dedicate it also to my newborn daughter, Eliana, whose anticipated arrival within days of my defense was the best incentive of all to finish!

Acknowledgments

First I would like to thank my research advisor, Dale Van Harlingen, for his patience, support and guidance, and for allowing me the latitude to pursue the research of which this thesis is a product. I also thank all the members of the DVH group that helped me in so many ways over the years. Special thanks also goes to Ismardo Bonalde for sharing his knowledge of dilution refrigerators, tunnel diode oscillators, and for working with me on the design and operation this experiment. Thanks to Elbert Chia for helping us run the system, and for asking questions that forced me think hard about the most fundamental issues. Thanks to Prof. Myron Salamon for helping us interpret our results, and to Cliff and Spencer in the machine shop for making many of the parts for the system.

Lastly, I gratefully acknowledge the support of the National Science Foundation under award number NSF DMR97-05695 and, through its Science and Technology Center for Superconductivity under award number STC DMR91-20000.

Table of Contents

1 Review of Experimental Techniques

In this chapter I will review a number of experimental techniques which have been used successfully to measure the penetration depth of superconductors. Since the experiments described in this thesis use a self-inductive tunnel diode oscillator technique, I will start with a fairly detailed discussion of oscillator measurements of superconducting samples. I will also discuss the techniques of mutual inductance, microwave surface impedance, torque magnetometry and Josephson junction modulation.

1.1 Self-Inductive Resonant Oscillator Techniques

One of the most useful devices, for many different kinds of measurements, is the resonant oscillator. The technique is quite simple in its design. An oscillation is established whose frequency can be made to depend on the physical quantity under investigation with a known relationship. The frequency can be measured with great precision simply by counting the number of cycles of the oscillation, and this can be converted to a precise value of the physical quantity in question.

Perhaps the best known example of the oscillator is the use of a pendulum to measure the acceleration due to gravity. If the length L of the pendulum is known, the frequency of oscillation $\omega = \sqrt{g/L}$ gives the acceleration. A very useful oscillator technique for solid state physics employs an electronic rather than mechanical resonance. An inductor-capacitor (LC) resonant circuit is constructed, and provided with a source of gain in a positive feedback configuration. The result is an oscillation at the resonant frequency of the LC circuit. By rendering the inductance or capacitance sensitive to a physical property of a sample, such as

dielectric constant or magnetic susceptibility, the resonant frequency will shift with changes to these properties.

There are a number of advantages of electronic oscillators over their mechanical analogs. The frequency can be made significantly higher, which allows for a precise measurement of frequency in a shorter time interval. These higher frequencies are accompanied by sharper resonance (greater quality factor, Q) which contributes to a stable and sensitive frequency response. If designed and constructed well, electronic oscillators can be made fairly insensitive to mechanical and electrical disturbances, and to other environmental factors as well.

In this thesis we will be primarily interested in the measurement of magnetic susceptibility of a solid state sample–specifically in the susceptibility of a superconductor, which will be proportional to its magnetic penetration depth. One of the earliest reports of such a measurement was by Schawlow and Devlin[1], who used a parallel LC oscillator to measure the temperature dependence of the penetration depth, $\lambda(T)$, for a rod-shaped single crystal of tin. The sample was placed inside the inductive coil of the oscillator, where it was subject to the magnetic fields generated therein by the oscillating current in the coil. The resonant frequency of a parallel oscillator is given by

$$f = \frac{1}{2\pi}\frac{1}{\sqrt{LC}}. \tag{1.1}$$

A small change δL in the inductance due the changes in λ of the sample will result in a relative shift δf in the resonant frequency

$$\frac{\delta f}{f} = \frac{1}{2}\frac{\delta L}{L}. \tag{1.2}$$

Using a simple relation for their cylindrical sample, that the $\delta L / L = \delta\lambda \cdot C / A$, where C is the sample circumference and A is the cross sectional area of the coil, they determine the penetration depth as

$$\delta\lambda = (A / \pi r)\delta f / f \,, \tag{1.3}$$

where r is the radius of the sample rod, and A is the cross sectional area between the sample and the coil. It is difficult in practice to measure A accurately, but a reasonable value can be obtained by calibrating with samples of different size. It is noteworthy that while this will affect the conversion from frequency (Hz) to units of length (Å), the functional dependence of $\delta\lambda$ on an independent parameter, such as temperature, is not affected by uncertainty in the value of A. In general the penetration depth will be related to the frequency by a factor, G, which depends only on the geometry of the sample and the coil

$$\delta\lambda = G\delta f \,. \tag{1.4}$$

Schawlow and Devlin's oscillator was constructed using a vacuum tube amplifier, at room temperature as the gain mechanism. The inductor, capacitor and sample were all at low temperature, immersed in liquid helium. The oscillation frequency was about 100 kHz, quite low for this type of application, where frequencies in the MHz range are more typical. For a tin crystal sample with diameter 7.4 mm, the frequency shift between T>Tc and T = 3.6 K was about 350 Hz, or ~0.3%. The resolution was determined by the stability of the oscillator, which would hold steady to within 1-2 ppm/hr (0.1-0.2 Hz/hr).

Schawlow and Devlin's technique includes most of the features used in subsequent resonant oscillator experiments. There were several refinements incorporated by experimenters in later years. In 1966 Boghosian *et al*.[2] used a tunnel diode as the feedback mechanism for an oscillator which they used to measure the density, by way of the dielectric constant, of liquid

^{3}He under pressure. In this case the liquid He filled the space between the plates of the capacitor, thus changes in dielectric constant were measured through the change in capacitance, rather than inductance. The use of a tunnel diode as the gain mechanism improved the system in several ways. First the frequency of the circuit was made higher, ~10 MHz, allowing a measurement with greater relative precision. Second, due to the low power requirements of the tunnel diode, the entire circuit, except for power supply, was maintained in the low temperature part of the cryostat, contributing to improved short term stability of the oscillator of 0.2 ppm. Lastly, the higher frequency increases the $Q \sim f/\Delta f$, also contributing to improved sensitivity.

Figure 1.1 shows the IV curve for the tunnel diode used in our circuit (Germanium Power Devices model BD-3). The important feature of the tunnel diode is the region of negative differential resistance. The shape of this characteristic curve comes from a combination of ordinary exponential diode behavior and quantum mechanical tunneling across the diode depletion layer (see for example Chow[3]). The negative resistance, R_n (a negative quantity), characterizes the gain of a given tunnel diode: a diode with greater gain has a smaller magnitude of R_n.

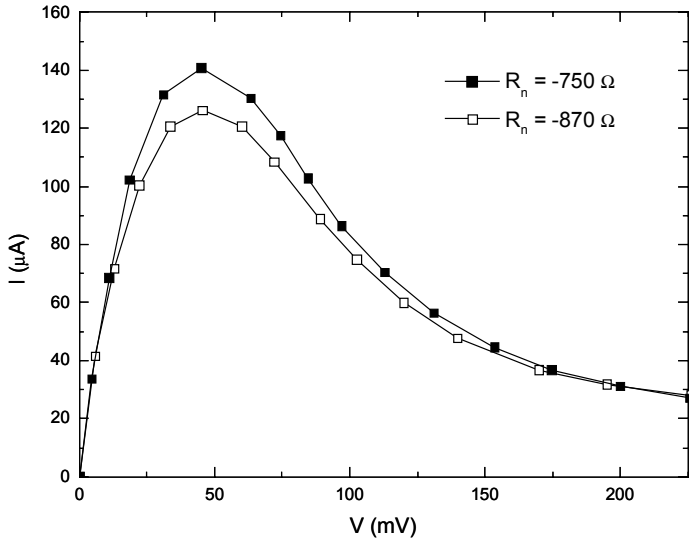

Figure 1.1
Measured current-voltage characteristic for two tunnel diodes (model BD-3) Variation among devices of the same model is typical.

When biased in the negative differential resistance region, and connected to a resonant circuit, the tunnel diode acts as a negative resistance for small ac signals converting some dc power to ac power in the form of oscillation of the tuned circuit. A typical arrangement of an LC tuned circuit is shown in Fig. 1.2.

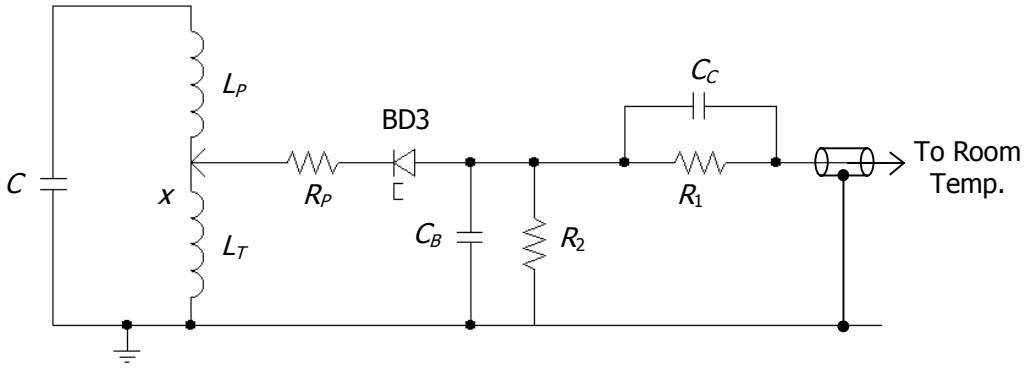

Figure 1.2

Low temperature electronics

Boghosian *et al*. found that some additional work was necessary to determine the frequency. Originally a simple transistor amplifier was used to increase the RF oscillation signal before counting the frequency. But it was found that this arrangement caused unwanted coupling between external parts of the apparatus and the oscillator frequency. A more satisfactory solution was found by using a mixer, with the 10 MHz clock signal from the frequency counter serving as the local oscillator. We use such an arrangement in our version of the tunnel diode oscillator, which is discussed in detail in the next chapter.

Another example of a tunnel diode oscillator measurement was done by Clover and Wolf[4] in 1970 to measure the paramagnetic susceptibility of several different materials. Frequencies from 3 to 55 MHz were possible in this oscillator system. Oscillator frequency was

stable to 1 ppm when immersed in liquid nitrogen, but only 10 ppm in liquid helium. The increased fluctuation is attributed to bubbles in the helium which could enter the coil. When the helium bath temperature was reduced below the lambda point, so that the boiling stopped, the fluctuations were reduced. The design of our system allows (actually, requires) that the coil and sample occupy a vacuum space, so the interfering effect of bubbles was not a problem. However, this arrangement lacks the very stable temperature which is achieved by immersing the oscillator circuit.

The publication of Van Degrift[5] describes the design and operation of a tunnel diode oscillator (TDO) with stability of 0.001 ppm at low temperatures. This treatment of precision TDO design served as our primary reference when putting together our oscillator. I will discuss the details of our implementation of this design in the next chapter. In principle, other techniques are possible for creating oscillators. For example, the gain mechanism could be provided by a FET amplifier. A number of FETs suitable for use at low temperatures are listed by Wagner *et al*.[6]

1.1.1 Calibrating an oscillator

One of the challenges of using the oscillator technique for experiments like the ones described here is the problem of calibration. Though glossed over in many discussions, making an accurate conversion from frequency response to changes in the physical quantity under study is often more difficult than it would first appear. In our case we must determine how changes in the frequency, in units of Hz, correspond to changes in penetration depth, in units of length. This calibration represents a simple multiplication of the raw data, so the functional dependence of $\Delta\lambda(T)$ will not be affected. However, other quantities calculated from $\Delta\lambda(T)$, in

particular the absolute magnitude of λ, are affected by this scale factor, so it is best to have an accurate calibration, if possible.

We need to know the relationship between the expulsion of the magnetic field by the sample and the change this causes in the inductance of the coil, and hence the frequency of the oscillator[7]. The energy of a coil of inductance L_0 carrying a current I is given by

$$U = \frac{1}{2} L_0 I^2 . \tag{1.5}$$

The energy is contained in the magnetic field and can be determined from the distribution of magnetic induction, $\mathbf{B}_0$, and magnetic field $\mathbf{H}_0$ for the empty coil:

$$U = \frac{1}{8\pi} \int_{\text{all space}} \mathbf{B}_0 \cdot \mathbf{H}_0 \, dV . \tag{1.6}$$

If a sample is placed inside the coil the fields become **B** and **H**, the inductance becomes L, and the change in energy is

$$\Delta U = \frac{1}{8\pi} \int_{\text{all space}} (\mathbf{B} \cdot \mathbf{H} - \mathbf{B}_0 \cdot \mathbf{H}_0) \, dV = \frac{1}{2} (L - L_0) I^2 . \tag{1.7}$$

It turns out that if the sources of magnetic field (the wires and current) are fixed, then this expression can be rewritten as

$$\Delta U = \frac{1}{2} \int_{V_s} \mathbf{M} \cdot \mathbf{B}_0 \, dV , \tag{1.8}$$

where **M** is the magnetization of the sample, and the integral extends only over the volume V_s of the sample (see for example, Jackson[8]). If an ellipsoidal sample with magnetic susceptibility χ_m is placed in a uniform magnetic field, $\mathbf{B}_0$, the magnetization induced in the sample will be

$$M = \frac{4\pi\chi_m}{1 + 4\pi N \chi_m} B_0 , \tag{1.9}$$

where N is the demagnetizing factor, which depends only on the shape of the sample ($N = 1/3$ for a sphere). The inductance of the empty coil can be found, in the long solenoid limit, from $\frac{1}{2} L_0 I^2 = B_0{}^2 V_c / 8\pi$, where V_c is the effective volume of the coil. The change in inductance, ΔL, relative to the empty coil, when the sample is placed inside is

$$\frac{\Delta L}{L_0} = \frac{4\pi\chi_m}{1 + 4\pi N\chi_m} \cdot \frac{V_s}{V_c}. \tag{1.10}$$

This will cause a change in frequency, according to Eq. 1.2, of

$$\frac{\Delta f}{f_0} = \frac{V_s}{2V_c} \cdot \frac{4\pi\chi_m}{1 + 4\pi N\chi_m}. \tag{1.11}$$

The idea of the calibration procedure is to measure the frequency shift, relative to an empty coil, when we insert a sample of known dimension and demagnetizing factor (a sphere of aluminum, diameter 0.79 mm, $N = 1/3$). The electromagnetic skin depth of the sphere is much less than its size, so we can take the sphere as perfectly screening, which corresponds to a susceptibility $\chi_m = -1/4\pi$. From the frequency shift we determine V_c from Eq. 1.10 as

$$V_c = 4\pi \frac{3}{2} \frac{V_s}{2} \frac{f_0}{\Delta f_{sphere}}. \tag{1.12}$$

Now the volume and shape of the real sample are measured from microscope photographs. The shape is approximated as an ellipsoid to determine the approximate demagnetizing factor. Using Eq. 1.10 again $\chi_m = -1/4\pi$, and with N appropriate to our approximated ellipsoid, and we find

$$\frac{\delta f}{f} = \frac{4\pi}{(1 - N)} \frac{\xi V_s}{2V_c} \tag{1.13}$$

The frequency shift we measure is $\delta f(T) = f(T) - f(T_{min})$. This represents small changes in the penetration of the field around the perimeter. The penetration depth is much smaller than the dimensions of the sample (except very close to T_c). We can picture the change in volume as a ribbon of excluded field around the perimeter of the sample (see Fig. 1.3), representing a volume

$$\delta V_s = Pt \cdot \delta\lambda \tag{1.14}$$

where t is the thickness of the (plate-like) sample and P is its perimeter. Using Eq. 1.2, putting in the expression for V_c and solving for $\delta\lambda$ we find

$$\delta\lambda = \frac{3}{2}\frac{V_{sphere}}{\Delta f_{sphere}}\frac{(1-N)}{Pt}\delta f \ . \tag{1.15}$$

Referring to Eq. 1.4 we would define $G = 3V_{sphere}(1 - N)/(2\Delta f_{sphere} Pt)$.

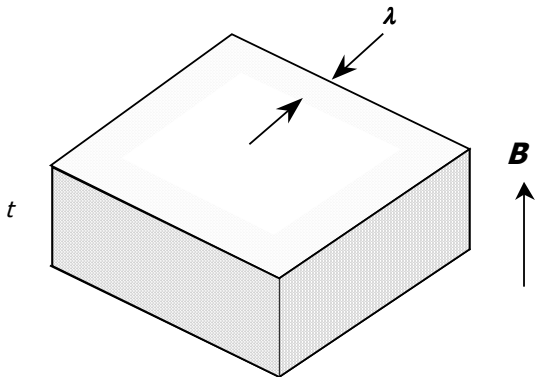

Figure 1.3
The sample in a magnetic field. The shaded volume is penetrated by the field. The thickness of the crystal is t.

This technique should work for ellipsoidal samples, in which the interior field is proportional to the applied field. However, for other shapes this is not true, and this technique will be accurate only to the extent that the shape of a given sample can be approximated as an ellipsoid. There is an alternative approach which does not require that we approximate the sample shape. We can determine G, which depends only on geometrical factors, for a sample of known response with the same shape as the sample we wish to study. We make G an adjustable

parameter and fit the data to the expected response. We can use the same G for the sample of unknown response which we wish to study. This has the advantage that we do not need to calculate G directly from the shape. One drawback is that if each sample has a different shape, then we need a different calibration sample for each real sample. In addition, depending on the shape of the sample, it may not be trivial to manufacture a calibration sample in the same shape. However, from our experience this technique works better for our samples than the other technique.

1.2 Microwave Surface Impedance

The microwave surface impedance (MSI) technique is fundamentally very similar to the oscillator techniques described in the first section. But because of the historical importance of this method in determining $\lambda(T)$ for the cuprates, which will be discussed in a later chapter, it warrants a more specific treatment.

The absorption of microwaves by a superconductor, at frequencies corresponding to less than the gap energy, depends on the density of quasiparticle states. At low temperatures, absorption in the superconducting state is extremely small. To amplify the effect of the absorption, a cavity can be constructed whose walls are made of, or coated with, the superconductor one wishes to study. Microwaves can then bounce back and forth many times off the surfaces, multiplying the absorption. The absorption is measured in terms of the Q of the cavity, which is measured as follows[9]: A pulse of rf power from an external source, at the cavity resonant frequency, is introduced by a coaxial cable into the cavity. The detected waves are observed on a fast oscilloscope, and the decay time, τ, is measured, giving $Q = \omega_0/\tau$. The value of Q can cover many orders of magnitude as a function of temperature, from as small as 10^4 to as large as 10^{12}. The resonant frequency, typically in the range of ~10 GHz, will also

vary with the temperature, because the variation of penetration depth will modify the effective size of the cavity.

It is not always convenient to make the entire cavity out of the superconductor under study. Sridhar *et al*.[9] devised a cavity, coated inside with superconducting Pb, maintained at 4.2 K by a helium bath. Into this cavity extends a sapphire rod which carries the sample–in this case a single crystal of high temperature superconductor. The cavity is under vacuum, allowing the sapphire rod and sample to be varied in temperature independently from the cavity walls. Meanwhile, the Pb coating on the walls, well below T_c, will have very small absorption, allowing the sample response to be detected independently.

In terms of the surface resistances R_{Pb} and R_s of the Pb and the sample, the Q of the cavity can be expressed as

$$Q = \frac{\alpha U_0}{\alpha R_{\mathrm{Pb}} + \beta R_s} \tag{1.16}$$

where U_0 is the energy stored in the electromagnetic field in the cavity, and α and β are constant factors which depend on the geometry of the cavity and sample. The change in penetration depth is given by

$$\begin{aligned} \Delta\lambda(T) &\equiv \lambda(T) - \lambda(T_0) \\ &= \zeta_s \Delta f(T) \end{aligned} \tag{1.17}$$

where ζ_s is another constant which depends on the geometry of the cavity and sample. The penetration depth is proportional to the surface reactance X_s. So from the measurement of Q and Δf the surface impedance $Z_s = R_s + iX_s$ can be determined. Determination of the geometrical factors has been accomplished in most cases by measuring a sample of known response, such as a well known superconductor, with a shape identical to the real sample. Using a substantially similar design, but with an improved "split ring" cavity configuration oscillating at 900 MHz,

Hardy *et al.*[10, 11] have reported resolution in measurements of $\Delta\lambda(T)$ on single crystals of YBCO of better than 1Å.

1.3 Mutual Inductance

A very useful technique for measuring the penetration depth is based on the screening of the mutual inductance which occurs when a superconducting film is placed between a driving and receiving coil. Such an experiment is described, for example, by Fiory and Hebard.[12] In this experiment the drive coil and the receiving coil, placed on opposite sides of the film, are each wound with half their turns clockwise and half counterclockwise (astatic). Other configurations are possible. For example, the coils can both be placed on the same side of the film, and different variations of coil winding are possible. However, the general principle remains the same: The magnetic field from the drive coil induces a screening current **K**(**r**) in the film, which depends on the complex impedance of the superconductor $Z(\omega) = R + iL$. For an oscillatory field and zero temperature the film would be purely inductive with a sheet kinetic inductance $i\omega L_K = m^* c^2 / n_s e^2 d_F$, where d_F is the film thickness. The measured inductive component is related to the in-plane penetration depth by the relation

$$L_K = \frac{4\pi\lambda_{\parallel}^2}{c^2 d_F}. \tag{1.18}$$

The kinetic inductance is determined from measurements of the in-phase and quadrature components of the mutual inductance between the drive and receive coils. By assuming values for complex impedance, Z, the distribution of screening currents, **K**(**r**), can be numerically calculated self-consistently in terms of the vector potential, **A**(**r**), produced by the particular arrangement of coils as follows:

$$\mathbf{K}(\mathbf{r}) = -\frac{i\omega}{Z} c^{-1} \left[\mathbf{A}(\mathbf{r}) + c^{-1} \int_{film} \frac{\mathbf{K}(\mathbf{r}')}{|\mathbf{r} - \mathbf{r}'|} d\mathbf{r}' \right]. \quad (1.19)$$

This simulation is performed for various values of L and R, and the mutual inductance is calculated. A lookup table is constructed which then allows the values of L and R to be deduced from measurements of the mutual inductance.

There are a number of advantages of this technique. First it allows non-destructive testing of unpatterned films, making it a convenient tool for characterizing a film prior to patterning it for device fabrication. Second, the technique allows for a wide range of different frequencies to be used, from ~10 Hz up to perhaps 10 MHz, with a value around 10 kHz typical. Unlike the oscillator technique which requires a modification of the circuit to change the frequency, the frequency can be changed with the turn of a knob in the mutual inductance experiment. Another advantage is that if the geometry can be accurately determined or calculated, there are no adjustable parameters required to determine numerical values for λ. One disadvantage is the requirement that the sample be in the form of a thin film with a fairly large area. While it is possible to grow high quality thin films of many of the cuprates, there are materials for which high quality samples are available only in the form of small crystals (Sr_2RuO_4, to name just one). While it might be possible to adapt the mutual inductance technique to this form, it is not as convenient as a thin film. To give a recent example of this technique, Paget *et al*.[13] made measurements of the penetration depth as a function of temperature for films of the cuprate $La_{2-x}Sr_xCuO_4$. They report a noise level in their measurement of $\lambda(T)$ of 10 Å.

1.4 SQUID Magnetometry

One of the most valuable tools in low temperature physics is the superconducting quantum interference device (SQUID), an exquisitely sensitive detector of magnetic flux. A SQUID is adaptable to a large number of different measurements. Not surprisingly, one such application is the measurement of magnetic flux excluded by a superconductor, *i.e*. the penetration depth. Just one example of this technique is the measurement of the temperature dependence of the penetration depth of the heavy fermion superconductor, UBe_{13}, by Gross *et al*.[14] Here the SQUID is configured in a bridge circuit using coils and wire made entirely of superconducting Nb. (See Fig. 1.4) Because the flux enclosed by a loop of superconductor is trapped inside, the wires and coils act as a so-called flux transformer. Currents are established by applying a small field to coils L_1 and L'_1 using copper coils L_p and L'_p. The currents divide among the coils according to the inductance of each, and some of the current flows through coils L_s, coupled to the SQUID, and L_2 and L'_2 containing the sample, and a reference sample of Sn. The change in the inductance in coil L_2 as a function of the penetration depth of the UBe_{13} sample is the same as in the oscillator technique. In this case the change in inductance is detected as a change in current flowing through coil L_s coupled to the SQUID. One of the principle advantages of the SQUID technique is that the currents and magnetic fields are all dc. The behavior of the penetration depth has been shown to have some dependence on high frequencies for certain heavy fermion superconductors,[15, 16] and in these cases the SQUID technique is most appropriate.

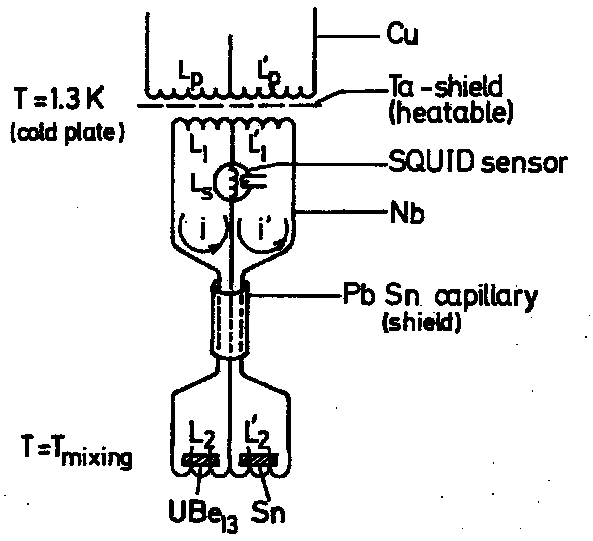

Figure 1.4
Superconducting SQUID bridge circuit used by Gross *et al.*[14]

1.5 Torque Magnetometry

A clever technique employing a torsion balance torque magnetometer[17] has been used recently by Waldmann *et al.*[18] to measure $\lambda(T)$ and $\lambda(0)$ for BSCCO based upon the magnetization of the sample in the vortex lattice state. A single crystal of the cuprate superconductor BSCCO is placed in a magnetic field oriented perpendicular to the *ab*-planes of the crystal. The torque for a highly anisotropic material with magnetization $M_\perp$ perpendicular to the planes is

$$\tau = -\mu_0 V M_\perp H \sin\theta \tag{1.20}$$

where V is the volume of the sample, μ_0 is the permeability of free space and θ is the angle between the field and the planes. Hao and Clem[19] calculate the reversible magnetization of a superconductor as a function of applied magnetic field, H, when vortices are present in a field intermediate between the upper and lower critical fields, $H_{c1} < H < H_{c2}$. They show that the approximate London model, which predicts a linear relationship between magnetization, M, and $\ln(H)$, is quantitatively incorrect because the energy associated with the cores of the vortices must be included in the calculation of the magnetization. The exact behavior of M is

not linear with ln(H), but they find that in an intermediate region of field the curve is close to linear and the magnetization due to the vortex lattice can be well approximated by

$$M_{\perp} = \frac{\alpha \Phi_0}{8\pi\mu_0\lambda_{ab}^2} \ln \frac{\beta H_{c2\perp}}{H\cos\theta}, \tag{1.21}$$

where $\alpha = 0.77$ and $\beta = 1.44$ are determined by fitting to the more exact theoretical results, and Φ_0 is the magnetic flux quantum. We see that the magnetization is proportional to λ^{-2} and can be extracted from the torque measurement.

The "pico-torquemeter" is constructed from a 22 mm long, 50 μm diameter PtW torsion wire with a plastic disk carrying the sample. Deflections in angle as small as $2 \cdot 10^{-6}$ degrees are measured by non-contact differential capacitance between a fixed plate and a gold plate on the torsion wire. Typical resolution is ~1 Å for sample weights of ~100 μg. Fields up to 16 T can be applied by a superconducting solenoid. The large fields allow the neglect of demagnetizing factors, since the sample is fully penetrated by vortices.

1.6 Muon Spin Relaxation

One of the most important of the modern techniques for measuring the penetration depth in superconductors is positive muon spin relaxation (μSR). The experiment is performed as follows: The superconducting sample is cooled in a magnetic field between H_{c1} and H_{c2}, where H_{c1} and H_{c2} are the lower and upper critical fields, respectively, of the superconductor, such that a regular vortex lattice is formed inside the sample. The penetration depth λ characterizes the spatial extend of the field of a vortex. A beam of spin polarized muons is directed at the sample and the muons come to rest, one at a time, inside the sample. The state of the muon evolves in the local magnetic environment, its spin precessing in the field. The muon decays with an average lifetime of 2.2 μsec, emitting a positron preferentially along its

direction of spin. Detection of the emitted positron allows one to determine the polarization of the muon at the time of its decay. By building up a large sample of such decay events, the average distribution of magnetic fields inside the sample can be determined. From this distribution, by making certain assumptions about the vortex lattice, the penetration depth can be calculated.

The number of detected positrons as a function of time is given by

$$N(t) = N_0\{B + \exp(-t/\tau_\mu)[1 - A_0 P(t)]\} \tag{1.22}$$

where B is a time-independent background, $\tau_\mu = 2.2\ \mu$sec is the lifetime of the muon, $P(t)$ is the component of muon polarization in the direction of the detector. The polarization precesses in the local field B_{local} according to

$$P(t) = G_{xx}(t)\cos(\gamma_\mu B_{\text{local}} t + \phi) \tag{1.23}$$

where γ_μ is the gyromagnetic ratio of the muon and $G_{xx}(t)$ represents the polarization relaxation, for which it is usual to take a Gaussian approximation, $G_{xx}(t) = \exp(-\sigma^2 t^2/2)$. The width, σ, of this polarization decay distribution gives us λ through the relation $\lambda^2 = \frac{\Phi_0}{\sigma\sqrt{16\pi^3}}$. Physically, this result comes about as a root-mean-squared average of the field variations due to the vortex lattice.[20]

An important advantage of the μSR technique is that it measures bulk behavior, and is insensitive to surface properties, effects of shape, thermal expansion, multiple connectivity of the sample, etc. In addition, it allows an accurate absolute determination of λ. In contrast, the technique of microwave surface impedance, and other resonant techniques which measure the Meissner currents circulating on the sample's surface, can be more susceptible to surface effects. And they likewise do not allow an absolute determination of λ.

One might ask why anyone would use techniques other than μSR at all, given their shortcomings. The μSR technique has a number of significant disadvantages from which some other techniques, notably microwave surface impedance, do not suffer. A source of muons is required for the μSR technique, which requires the experiment to be performed at the site of a particle accelerator beam line. Such facilities are in heavy demand, which requires that they be shared among researchers from around the world. Experiments using the beam line must therefore be designed and built off site, transported to the beam line, and measurements taken in the short time allotted. Aside from such administrative issues, there is another important difference between μSR and microwave techniques. While microwave surface impedance cannot always accurately determine the absolute value of λ, it can measure *variations* of λ with much higher sensitivity than μSR. Also, while the theory used to extract λ from μSR measurements is well developed, there is a significant amount of modeling involved, and some results may depend on the details of the model. Other techniques are able to measure variations of λ directly.

The technique of μSR is more general than it might appear from the above treatment. In fact it provides a useful measurement of the magnetic properties of a wide variety of different material types. An important example is the measurement of μSR in superconductors in zero applied field. If the superconductor exhibits time-reversal symmetry breaking, spontaneous magnetic fields are predicted to appear within the material. Such effects have been observed in UPt_3[21], UBe_{13}[22] and Sr_2RuO_4[23], as I will discuss in more detail in a later chapter.

1.7 Josephson Junction Modulation

A unique technique has been used by Froehlich *et al*.[24] to measure the penetration depth and its variation with temperature in epitaxial films of YBCO. A grain-boundary Josephson junction is prepared. The critical current of this junction will be modulated by magnetic flux Φ passing through the junction according to the Fraunhofer diffraction-like expression

$$I_c(\Phi) = I_c(0)\frac{\sin \pi\Phi/\Phi_0}{\pi\Phi/\Phi_0} \tag{1.24}$$

where Φ_0 is the flux quantum. The flux is given by the product of the field H and the effective area of the junction which depends on the penetration depth of the material giving $\Phi = (t + 2\lambda)wH$, where t is the barrier thickness, and w is the width of the junction. Since the junction geometry is known, the penetration depth can be determined in a simple and direct way. In their paper, Froehlich *et al.* read the flux off at the flux values where the critical current has its maxima, at approximately $\Phi^n_{\max} = (n + \frac{1}{2})\Phi_0$. As temperature is varied, the flux value of the maxima can be followed to determine $\lambda(T)$.

The expression for $I_c(\Phi)$ assumes the width of the junction w is less than the Josephson penetration depth, λ_J. If this condition is not satisfied, then the effective area of the junction will no longer be temperature independent but will depend on the reduced junction width $w/\lambda_J(T)$. Froehlich *et al.* point out that this effect becomes less important as the higher values of n are chosen, *i.e.* lobes farther out on the diffraction pattern. A second assumption implicit in Eq. 1.24 is that the critical current density J_c is uniform across the junction. If this condition is not satisfied then measurements must be interpreted as $\Delta\lambda(T) = \lambda(T) - \lambda(0)$ rather than an absolute measurement. Finally, flux focusing effects can give a substantial error in the effective field applied to the junction. While an exact determination of this focusing effect is necessary

for an absolute measurement, the effect should be independent of temperature, and so once again allows a relative measurement.

References

1 A. L. Schawlow and G. E. Devlin, Physical Review **113**, 120 (1959).

2 C. Boghosian, H. Meyer, and E. Rives John, Physical Review **146**, 110 (1966).

3 W. F. Chow, *Principles of Tunnel Diode Circuits* (John Wiley & Sons, Inc., New York, 1969).

4 R. B. Clover and W. P. Wolf, Review of Scientific Instruments **41**, 617 (1970).

5 C. T. Van DeGrift, Review of Scientific Instruments **46**, 599 (1975).

6 R. R. Wagner, P. T. Anderson, and B. Bertman, Review of Scientific Instruments **41**, 917 (1970).

7 F. Habbal, G. E. Watson, and P. R. Elliston, Review of Scientific Instruments **46**, 192 (1975).

8 J. D. Jackson, *Classical Electrodynamics* (Wiley, New York, 1999).

9 S. Sridhar and W. L. Kennedy, Review of Scientific Instruments **59**, 531 (1988).

10 W. N. Hardy, D. A. Bonn, D. C. Morgan, *et al*., Physical Review Letters **70**, 3999 (1993).

11 D. A. Bonn, S. Kamal, K. Zhang, *et al*., Physical Review B **50**, 4051 (1994).

12 A. T. Fiory and A. F. Hebard, Applied Physics Letters **52**, 2165 (1988).

13 K. M. Paget, S. Guha, M. Z. Cieplak, *et al*., Physical Review B **59**, 641 (1999).

14 F. Gross, B. S. Chandrasekhar, D. Einzel, *et al*., Zeitschrift fur Physik B **64**, 175 (1986).

15 P. J. C. Signore, B. Andraka, M. W. Meisel, *et al*., Physical Review B **52**, 4446 (1995).

16 W. O. Putikka, P. J. Hirschfeld, and P. Wolfe, Physical Review B **41**, 7285 (1990).

17 F. Steinmeyer, R. Kleiner, P. Muller, *et al*., Europhysics Letters **25**, 459 (1994).

18 O. Waldmann, F. Steinmeyer, P. Muller, *et al*., Physical Review B **53**, 11825 (1996).

19 Z. Hao and J. R. Clem, Physical Review Letters **67**, 2371 (1991).

20 P. Pincus, A. C. Gossard, V. Jaccarino, *et al*., Physics Letters **13**, 21 (1964).

21 G. M. Luke, A. Keren, L. P. Le, *et al*., Physical Review Letters **71**, 1466 (1993).

22 G. M. Luke, L. P. Le, B. J. Sternlieb, *et al*., Physics Letters A **157**, 173 (1991).

23 G. M. Luke, Y. Fudamoto, K. M. Kojika, *et al*., Nature **394**, 558 (1998).

24 O. M. Froehlich, H. Schulze, R. Gross, *et al*., Physical Review B **50**, 13894 (1994).

2 Experimental Design

The principles of resonant oscillator measurements in general, and tunnel diode oscillators in particular were discussed in chapter 1. In this chapter I will discuss the details of the construction and performance of our tunnel diode oscillator system. We will first consider the design of the electronic oscillator circuit and then discuss the pieces that mechanically hold the system together.

In this experiment we measure the temperature dependence of the penetration depth in the temperature range from 1 K down to lowest temperature that can be attained in our ^{3}He-^{4}He dilution refrigerator (DR). Under the full heat load of the experiment, our DR can reach a temperature of approximately 30 mK. Our DR, an Oxford Instruments Kelvinox 25, has a rather modest cooling power of only 25 μW at 100 mK. The cooling power of a DR will drop as T^2,[1] so below 100 mK the cooling power drops rapidly. It is only through careful design that this low a temperature can be reached in a DR of this power. The dewar which houses the DR is surrounded by a dual-layer mu-metal shield which shields the experiment from the earth's field, to a level less than 1 mT. This prevents the effects of vortices becoming trapped in the sample as it cools below T_c.

Craig Van Degrift[2] conducted a systematic study of low temperature tunnel diode oscillators, and presents design specifications for a tunnel diode oscillator (TDO) with frequency stability of 0.001 ppm. Our experiment is modeled after the design described in this paper. One of the main advantages of a TDO over other methods of generating oscillations is the small size and low power requirements of the tunnel diode, which permit the oscillator circuit to be located in the low temperature portion of the apparatus–even immersed in liquid helium. Immersion, in particular, provides a very stable temperature environment for the

components of the oscillator, contributing to a very stable oscillation frequency. If the circuit cannot be immersed, as in our case, it is possible to use temperature control techniques to maintain a stable low temperature in the circuit.

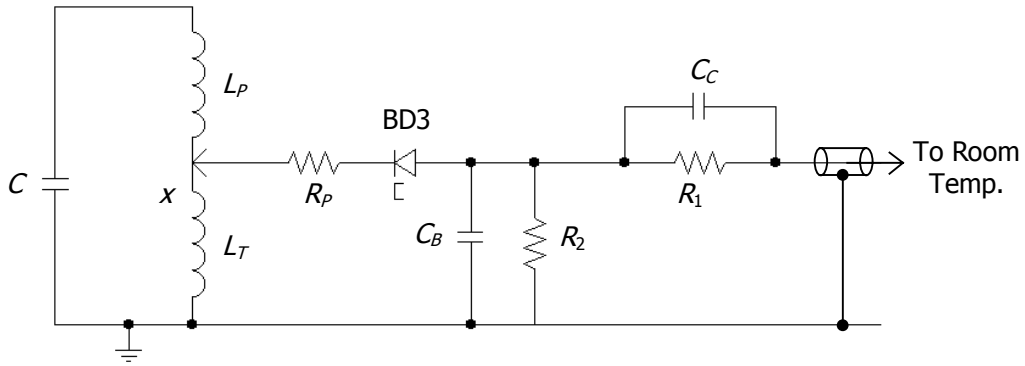

Figure 2.1

Schematic diagram of low temperature oscillator circuit. The circuit components used in our experiment are C = 100 pF, R_P = 300 Ω, C_B = 10 nF, R_2 = 300 Ω, C_c = 20 pF, R_1 = 1400 Ω

2.1 Tunnel Diode Oscillator Circuit Design

The design of the experiment is based directly on the design described by Craig Van Degrift[2]. The oscillator portion of the circuit, a parallel LC resonant circuit, is inside the cryostat, at low temperature. The gain required for oscillation is provided by a tunnel diode (Germanium Power Devices model BD-3).

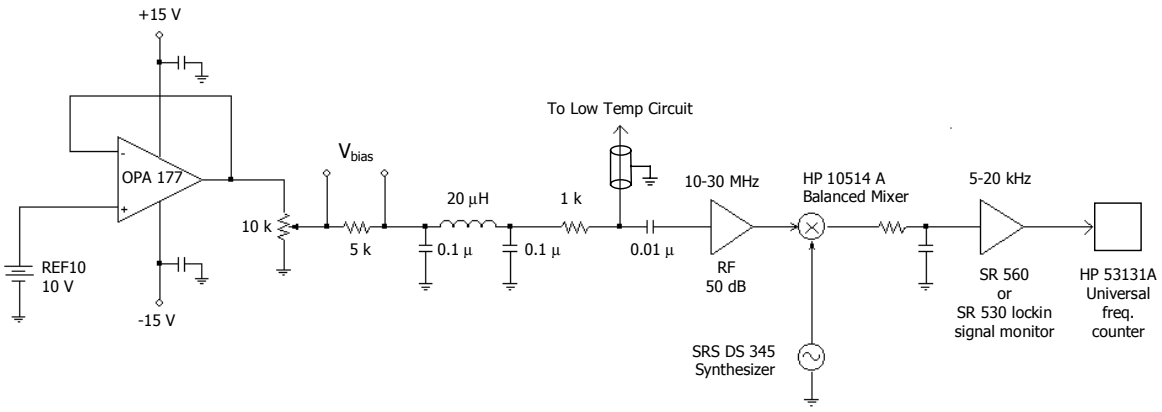

Figure 2.1

Schematic diagram of room temperature electronics.

The dc bias for the tunnel diode circuit is generated at room temperature by a semiconductor reference voltage source (Burr-Brown model REF10), which provides a very stable 10 V output. This voltage is buffered with a low noise op-amp and filtered before passing out to the cryostat through a semi-rigid coaxial cable. The rf oscillation signal (10-30 MHz) is carried back out on this same coax cable. The ac component is coupled through a capacitor to an rf amplifier (Trontech, Inc. model W50ATC) and then to a balanced mixer (Hewlett-Packard model 10514A). The frequency output from the mixer is the difference between the signal frequency and the frequency of the local oscillator (LO) signal from a synthesizer (Stanford Research Systems model DS345). The LO frequency is adjusted to set the mixer output frequency to a convenient value, usually 10-20 kHz. The signal passes through an audio frequency amplifier, a bandpass filter and then to a universal frequency counter (Hewlett-Packard model 53131A). The frequency counter is equipped with an optional high stability time base, which provides stability of 1 ppb. This 10 MHz time base signal is also used to generate the synthesized local oscillator signal.

We have found it very effective to use the input stage of a lockin amplifier as the audio amplifier. The usual lockin output is not used, instead an output on the back of the instrument provides access to the preamplified, filtered signal, before it goes to the lockin stage of the amplifier. The filter is a bandpass type centered at the lockin reference frequency, with a bandwidth of 1/5 of the reference frequency. The center frequency can conveniently be adjusted by adjusting the reference frequency input. The signal frequency should stay within the pass band as it shifts due to the temperature dependence of the sample. The frequency from the mixer is typically ~10 kHz, so the bandwidth is ~2 kHz. If the frequency shift over the temperature range of interest is greater than 2 kHz, then the LO frequency and lockin reference frequency can be easily adjusted to a different value.

2.2 Mechanical Design

The mechanical design of the low temperature part of the system is constrained primarily by the requirement that different portions be maintained at different temperatures, and by the limited cooling power of the dilution refrigerator. The system can be divided into three parts. The cold finger, which carries the sample must allow the temperature to vary from the base temperature of the fridge up to about 1 K. The electronics, which includes the tunnel diode as well as the capacitors, resistors, and tap coil which form most of the oscillator circuit, must be at a constant temperature because the frequency will change when the temperature of these components changes. Lastly, the primary coil must also be at constant temperature. In our design, the coil can be maintained at a different temperature from the electronics. I will describe the construction of each of these parts in detail.

The cold finger is made in three pieces. The main portion is made from a single piece of gold-plated, oxygen free high conductivity (OFHC) copper. It has a round flat plate which

covers the entire bottom mounting surface of the mixing chamber of the fridge, where it is held with stainless steel screws threaded into tapped holes in the mixing chamber. A cylindrical finger extends from the center of the flat part. Attached to the end of the large finger with silver conducting epoxy is a smaller diameter finger of OFHC copper. At the end of this smaller finger, a 1.25 mm diameter sapphire rod is affixed with Stycast 1266 epoxy. The sample is held on the end of the sapphire rod with a small amount of silicone vacuum grease or GE varnish. Near the end of the small copper finger is a small chamber formed by hollowing out a portion of the copper and covered by a cylindrical shield. Inside this chamber is a calibrated RuO_2 chip resistor (called "RuO2 A") which we use to measure the temperature of the sample. This thermometer was calibrated against two different calibrated resistor thermometers and against a ^{60}Co nuclear orientation thermometer. Whether the temperature of the thermometer on the small copper finger, and the sample on the end of the sapphire rod are the same, of course, depends on establishing thermal equilibrium. I will discuss this in more detail later in this chapter.

The primary coil is made from 0.0025" diameter (42 gauge) copper wire. It is made by hand in the following way: A drill bit is selected with the desired inner diameter of the finished coil. A small piece of very thin Mylar is wrapped several times around the shank of the drill bit. Then two pieces of wire are wrapped side-by-side over the Mylar with the windings packed close together until the desired length is reached. A small amount of clear Stycast 1266 epoxy is applied to the wires and the curing accelerated by careful application of heat with a heat gun. When the glue is nearly fully cured, one of the two wires is carefully unwound, leaving behind a single wire which forms the coil with uniform spacing between turns equal to one wire diameter. The advantage of this technique over simply winding the turns closely packed

together is that the shunting capacitance between adjacent turns is significantly reduced. Several additional thin layers of Stycast are applied to the coil to strengthen it before the coil and Mylar are then slid off the end of the drill bit. The Mylar is peeled away from the inside of the coil, leaving the coil as a free-standing piece of wire and Stycast.

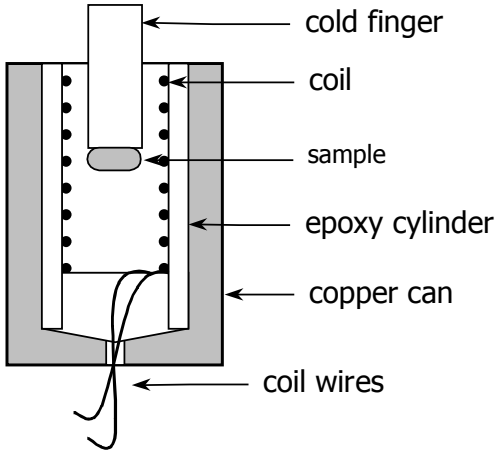

Figure 2.1
The primary coil with cold finger and sample inserted.

Stycast 1266 is cast into a solid cylinder, and this is machined into a small tube. The coil, with only a thin layer of hardened Stycast supporting it, is glued into the Stycast tube, and the tube is then glued inside a cylindrical copper can with more Stycast. This shields it from any stray signals and also allows the temperature of the coil to be regulated.

The copper can containing the primary coil is glued with GE varnish into a small recess in a round flange made from gold-plated OFHC copper. This flange has a threaded hole which allows a screw to affix a silicon diode thermometer and a small heater to measure and control the temperature of the flange and coil. The coil is controlled at a constant temperature usually from 1.4 K up to a few Kelvin using a Lakeshore model 340 temperature controller, which is capable of controlling within ~0.2 mK of the setpoint. In order to provide a source of cooling for the coil, a heavy copper wire is connected through a copper rod to the 1 K pot of the dilution fridge and held to the coil flange with a screw at the same point where the thermometer and heater are attached.

The sample, on the end of the cold finger's sapphire rod, must be positioned in the center of the primary coil. A hollow tube is used to hold and align the coil flange in position relative to the cold finger. The tube is made from Vespel SP-22 (available from DuPont) which is selected for its extremely low thermal conductivity at low temperatures. To maximize the thermal resistance, the Vespel support tube is machined to 0.050" wall thickness. It is constructed from three separate pieces which are nested, one inside the other, and connected with brass flanges on their ends as shown in Fig. 2.2. This arrangement allows the length of the tube to double back on itself, adding to the thermal path length without adding to the overall length of the part. We have taken great care to minimize the amount of heat which can flow from the coil (at a temperature of several Kelvin) to the other end of the Vespel support tube, which is fixed to the cold finger and mixing chamber (at a temperature down to 30 mK). Any excess heat load on the mixing chamber will raise the temperature, and we will be unable to reach the lowest temperatures needed for the experiment.

The oscillator electronics is housed inside a small gold-plated copper can constructed such that half of the cylinder can be removed, allowing adjustment of the circuit inside. The circuit itself is held on both sides of a piece of copper plate, which stands vertically inside the housing. Connections between components on opposite sides of the plate pass through drilled holes. The wires are secured in the holes, thermally anchored to, but electrically insulated from the plate, using black Stycast 2850 epoxy. The copper plate is the ground for the circuit. Several pins made from thick copper wire are soldered to the plate using Sn-Ag solder (97% Sn, 3% Ag, Kester Lead-Free solder), which has a lower superconducting temperature (3.7 K) than ordinary Pb-Sn solder (7.3 K). Ground connections in the circuit are soldered to these pins using Pb-Sn solder. A short piece of semi-rigid coax with an SMA coaxial connector on its free

end is soldered into the fixed side of the circuit housing. The shield of the coax anchors the ground for the housing and the center conductor carries the signal and bias voltage. The center conductor of the coax is exposed inside the housing and passes from behind the copper plate through a hole to the front and is soldered to the circuit. A heavy copper wire is soldered to the housing at the point where the coax enters, and is soldered to the circuit, providing both electrical ground and thermal anchoring of the circuit to the housing. To further increase the thermal anchoring of the copper plate a copper braid is attached to the plate at one end with a small screw. The other end is connected with a screw to the outside of the cylindrical enclosure. The wires from the primary coil pass through a small copper tube, through a hole in the top of the electronics housing and connect to the oscillator circuit with a tiny two-pin connector (Microtech Inc.).

The circuit employs a tapped inductor coil. While the original paper by Van Degrift used a single coil with a tap connection in the middle, we have found it easier to make two separate coils. The tap coil is wound on and glued permanently to a piece of quartz tubing, and held by a small nylon spacer inside a copper can in the electronic circuit housing. This tiny can is fixed to the copper plate with an 0-80 screw.

The electronics housing is held beneath the coil flange by three spacers made of graphite, each with a small cardboard washer. These insulate the electronics thermally from the coil flange, allowing them to be controlled at different temperatures. The electronics temperature is controlled by the Lakeshore controller using a calibrated Cernox thermometer and small heater. Because heat is also generated within the oscillator circuit, the electronics is often significantly warmer than the coil flange. If the temperature of the coil flange rises too high, excess heat will be conducted to the mixing chamber through the Vespel support, raising

the mixing chamber temperature. To provide cooling for the electronics, a heavy copper wire conducts heat from the electronics to the top plate of the vacuum can, which is at the helium bath temperature of 4.2 K.

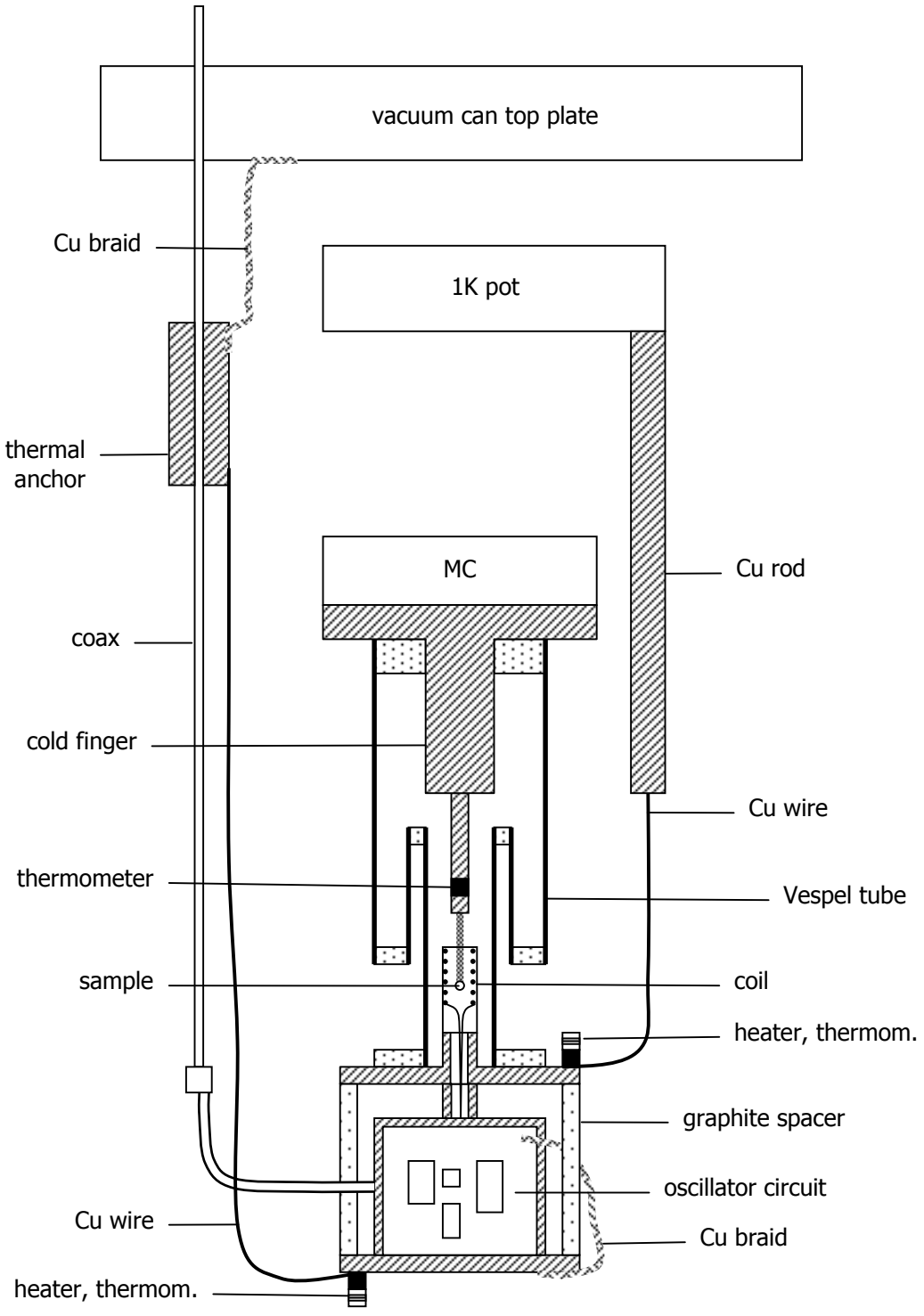

Figure 2.2

Schematic of tunnel diode oscillator system. MC is the mixing chamber of the dilution refrigerator. The 1K pot and vacuum can top plate are also shown. For clarity, the vacuum can itself is not shown.

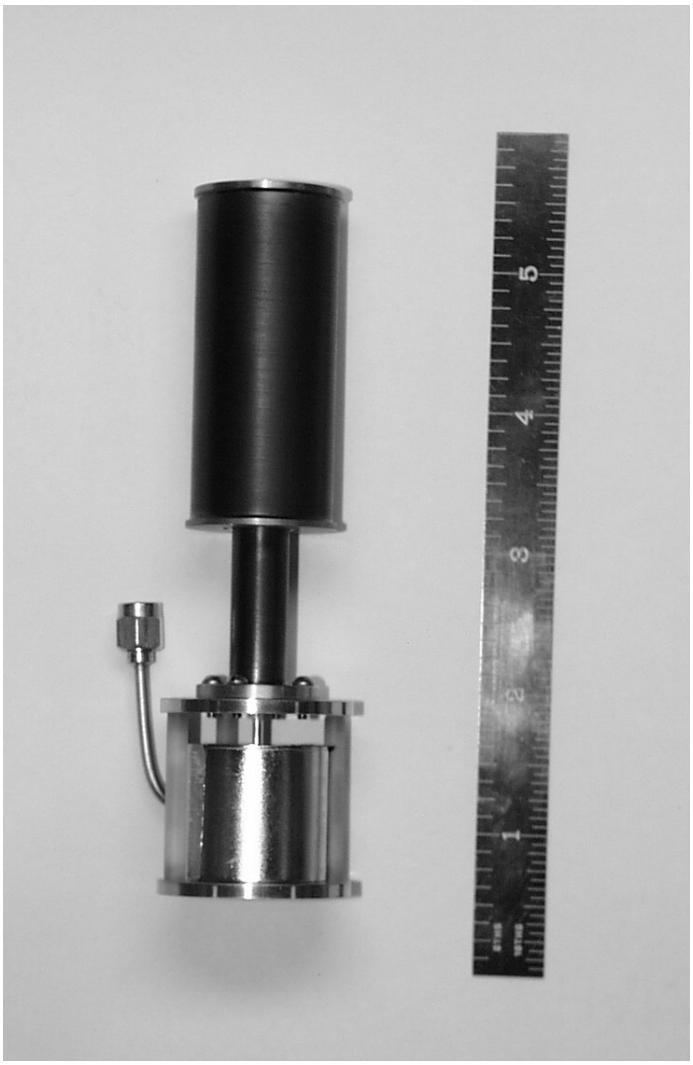

(a)

(b)

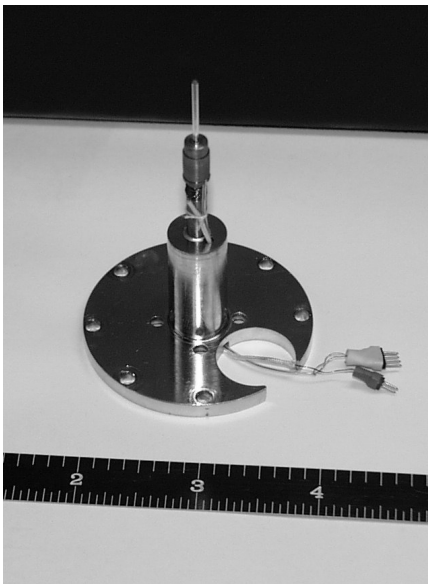

(c)

Figure 2.3

Photographs of tunnel diode oscillator system. (a) electronics and coil attached to Vespel tube (b) electronics and coil alone (c) cold finger

2.2.1 Thermal Conductivity

There are two aspects of the design of our system where the thermal conductivity of materials is important. In one case we want the conductivity as high as possible, and in the other as low as possible. The thermometer resides on the copper portion of the cold finger where it can be relied upon to accurately reflect the temperature of the mixing chamber. But the sample is located at the tip of the sapphire rod. Thus we rely on the thermal conductivity of the sapphire rod to maintain equilibrium between the thermometer and sample. At temperatures below about 100 mK, the thermal conductivity of most electrically insulating materials become very small and it may require a long time to establish thermal equilibrium. A single crystal of high purity sapphire of the type used for our cold finger has very high thermal conductivity compared to most insulators.

Using data from the low temperature book by Pobell[3], we calculate the thermal conductivity of our sapphire rod at 100 mK to be approximately 4 nW/K. The heat delivered to the sample by thermal radiation is somewhat difficult to estimate. To determine whether the thermal conductivity of the sapphire would be adequate to cool samples to temperatures near the mixing chamber temperature, we affixed a second RuO_2 resistor chip thermometer to the end of the sapphire rod and performed sweeps of the mixing chamber temperature. To the extent that the thermometer on the end of the sapphire rod agreed with that on the copper part of the cold finger, it can be assumed that the sample will be in thermal equilibrium. The thermometers agree very well above 100 mK. Below this temperature it required many minutes (at least) for the sample to come to equilibrium.

Sapphire has several advantageous characteristics as a cold finger material. It has no magnetic susceptibility (at least in this temperature range) and is electrically insulating. The

latter is useful because at the high frequencies, at which our coil oscillates, eddy current heating can be quite significant. However, in order to improve the thermal conductivity, we judged it better to replace the sapphire rod with high purity (99.999%) silver. Silver has low-temperature conductivity several orders of magnitude greater than sapphire at these temperatures. To minimize the effect of eddy current heating, the 1.25 mm diameter sapphire rod was replaced with nine pieces of 0.25 mm silver wire. Conducting silver epoxy was used to attach the silver wires to the copper cold finger. Each wire was individually coated with an insulating layer of Stycast 1266 to eliminate conducting paths of large area. The bundle of wires is encapsulated in Stycast 1266 to form a rigid rod 1.25 mm in diameter with the ends of the wires exposed, allowing the sample to make thermal contact.

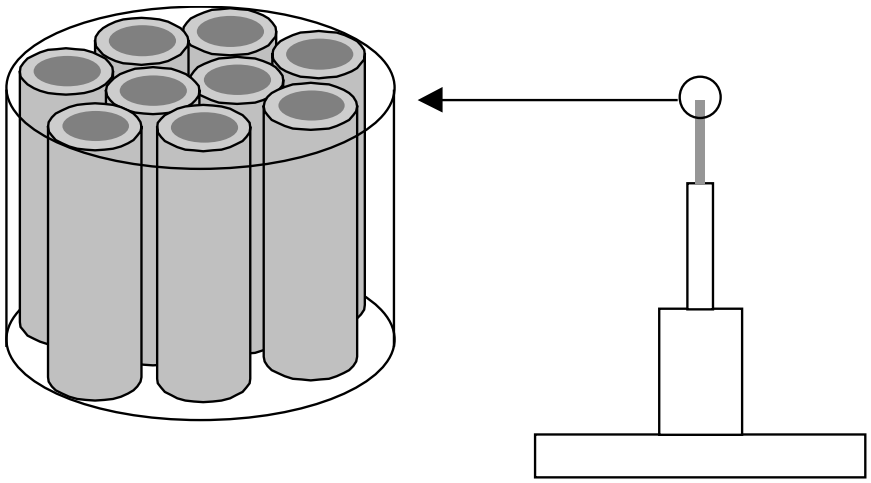

Figure 2.1
The cold finger. A detail of the silver wire bundle is shown.

2.3 Calibration

As discussed in section 1.1.1, we need to determine the factor *G* that converts from frequency to penetration depth. We have (at least) two different ways of calibrating our system.

The first is to measure the frequency shift when a sphere is inserted into the coil. The second is to make a sample of known response in the same shape as the real sample.

For consistency, we performed the first technique at 4.2 K, with exchange gas in the vacuum space to maintain thermal equilibrium with the main helium bath. The oscillator system is assembled as usual, but without a sample, and cooled in the usual way to 4.2 K. Oscillation is established and the resonant frequency is noted. The system is then warmed to room temperature and the process repeated, but this time with a 1/32 in. (0.79 mm) diameter aluminum sphere installed as a sample. At 4.2 K the aluminum is well above its superconducting transition temperature, but the ordinary electromagnetic skin depth serves to screen the high frequency magnetic field from the interior. The increase in resonant frequency, relative to the empty coil, is recorded. Let us call this frequency difference Δf_{sphere}. We now use Eq. 1.12 to determine V_c. As discussed in Ch. 1 this technique will be accurate only for ellipsoidal samples. A typical value is $G = 17$, obtained for a typical sample (C82A1-2a). By comparing $\Delta\lambda(T)$ with values of $\lambda(0)$ from the literature, it appeared that this calibration technique severely overestimates the change in penetration depth for our samples. We turned then to the second technique.

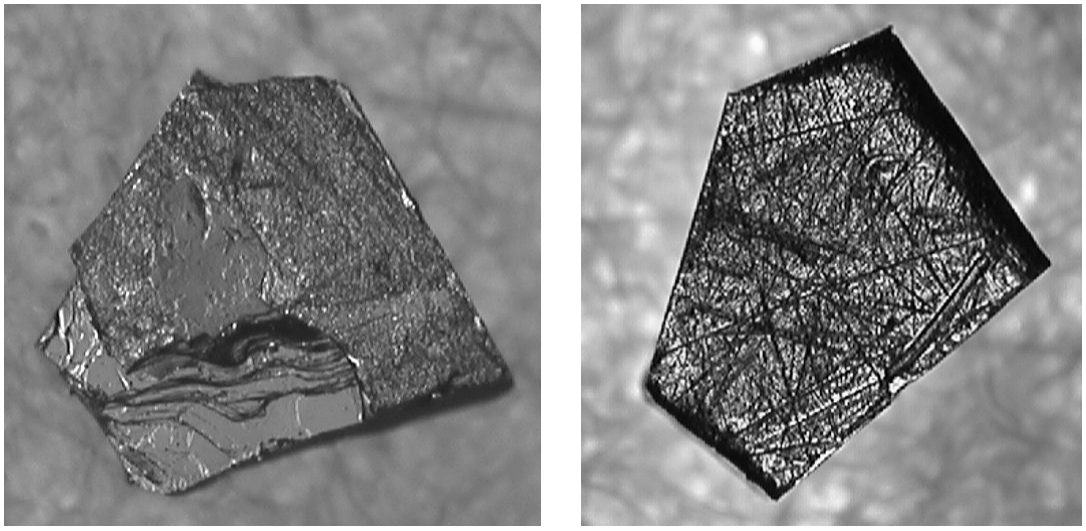

C82A1-2a Al#1

Figure 2.1

Comparison of the shapes of SRO sample C82A1-2a and high purity aluminum sample Al#1.

A small piece of high purity Al wire (99.9995%) was ground on silicon carbide sandpaper and emery paper to form a rectangular plate with the same thickness as one of the samples (sample C82A1-2a). Then, by measuring the dimensions under a microscope, the plate was cut into the approximate shape and size of the sample with a razor blade. We called the aluminum sample Al #1.

The penetration depth of a nonlocal superconductor, such as aluminum, has a temperature dependence as follows:[4]

$$\frac{\lambda(T)}{\lambda(0)} = \left[\frac{\Delta(T)}{\Delta(0)}\tanh\left(\frac{\Delta(T)}{2k_B T}\right)\right]^{-1/3}. \tag{2.1}$$

The temperature dependence of the energy gap can be approximated by the weak coupling interpolation formula

$$\frac{\Delta(T)}{\Delta(0)} = \tanh\left(\frac{\pi k_B T}{\Delta(0)}\sqrt{0.953\left(\frac{T_c}{T}-1\right)}\right). \tag{2.2}$$

Figure 2.2 shows the agreement between the theory and the data for aluminum for the superfluid fraction, $n_s(T)/n_s(0) = \lambda_L(0)^2/\lambda_L(T)^2$. The geometry factor $G = 2.5$ is the value for which the data best agrees with the theoretical curve. To give an idea of the sensitivity of the fit to the scale factor, curves are shown with G adjusted ±10%.

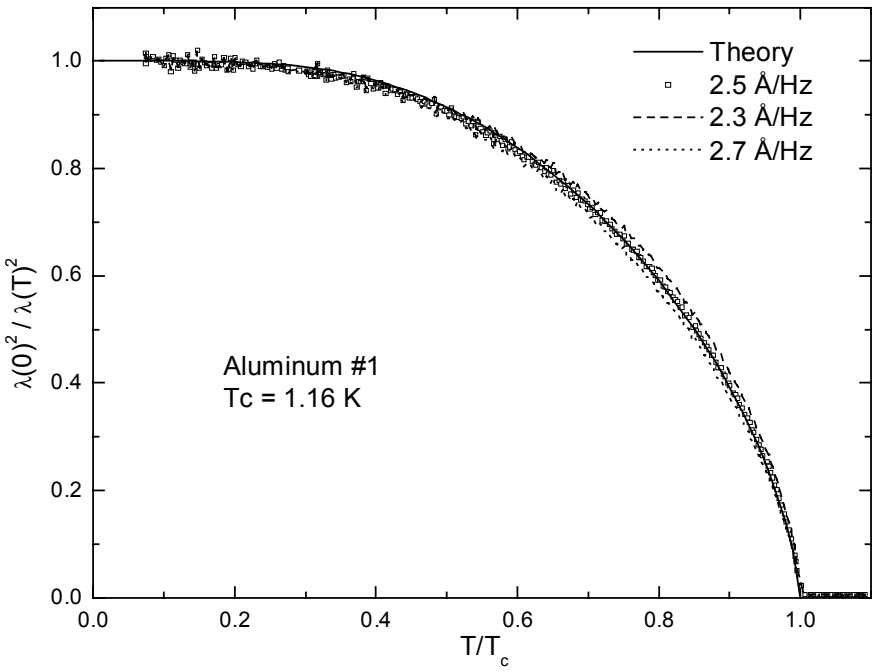

Figure 2.2
Superfluid fraction of Al#1, using $G = 2.5$, normalized to $\lambda(0) =$ 500 Å. The line is the theoretical curve.

2.4 Performance

In order to be able to accurately determine the temperature dependence of the penetration depth using this technique, we must be assured that the systematic errors in the measurement are reduced sufficiently. This places stringent requirements on the design.

The most important criterion is the stability of the frequency measurement. For a number of reasons, the total change in frequency is very small. First is the size of the samples. To fit on the end of the sapphire cold finger samples must be less than 1 mm square. The typical thickness of our samples is several hundred microns at most, depending on the material. Since the shift in inductance of the coil is proportional to the change in its effective volume,

these tiny samples provide a smaller signal than would larger samples. The second reason is that for the cuprate materials our measurements are taking place well below T_c. Since the penetration depth has its largest change around T_c, this means the signal is inherently small in our temperature range. Even assuming the linear behavior in BSCCO, as reported by Lee *et al*.[5] continues to hold below 1 K, the total change in λ from 1 K down to 30 mK would be ~10 Å. For our samples, this would correspond to a frequency shift of ~100 mHz. In order to get a sensitive measurement of $\lambda(T)$ we would therefore need frequency stability on the order of 10 mHz.

The overall frequency stability is a function of several variables. Most important, and at the same time easiest to achieve is the stability of the local oscillator. The HP 53131A frequency counter has a high stability 10 MHz time base, with stability of 1 ppb. This time base is also used to drive the synthesizer, giving it the same stability. The frequency will also vary with bias voltage because the capacitance of the tunnel diode is voltage dependent. We estimate the necessary stability at 2 ppm. The bias voltage is approximately 2 V, so we require stability of ~4 μV. By carefully constructing the room temperature electronics, we are able to achieve this stability. Finally, the frequency will drift with changes in the temperature of the oscillator circuit and the primary coil. The circuit is sensitive to temperature fluctuations at ~100 Hz/K. For 10 mHz resolution we require temperature stability of ~0.1 mK. The stability requirements for the coil temperature are less stringent. Frequency varies at a rate of ~5 Hz/K for fluctuations of the coil, so it needs to be stable to within ~2 mK. Both of these temperature stability requirements are accomplished by controlling with temperature sensors and heaters using a very good temperature controller (Lakeshore 340).

References

1 O. V. Lounasmaa, *Experimental Principles and Methods Below 1K* (Academic Press, New York, 1974).

2 C. T. Van DeGrift, Review of Scientific Instruments **46**, 599 (1975).

3 F. Pobell, *Matter and Methods at Low Temperatures* (Springer-Verlag, Berlin, New York, 1996).

4 P. M. Tedrow, G. Faraci, and R. Meservey, Physical Review B **4**, 74 (1971).

5 S.-F. Lee, D. C. Morgan, R. J. Ormeno, *et al*., Physical Review Letters **77**, 735 (1996).

3 Penetration Depth in Unconventional Superconductors

In this chapter I will discuss the behavior of the penetration depth in unconventional superconductors. I will begin by discussing the BCS treatment of conventional superconductors following closely the treatment by Tinkham[1]. I will then contrast the behavior of unconventional materials.

3.1 Conventional Superconductors

To determine magnetic penetration depth of a superconductor, we must understand how the electrons respond to electromagnetic field, *i.e*. a magnetic vector potential **A**, where the field $\mathbf{B} = \nabla \times \mathbf{A}$. The current density is simply proportional to the velocity **v** of the electrons, and their density n: $\mathbf{J} = ne\mathbf{v}$. The velocity is determined by to the canonical momentum $\mathbf{p} = m\mathbf{v} - \frac{e}{c}\mathbf{A}$. The resulting current becomes

$$\begin{aligned} \mathbf{J} &= ne\left(\frac{\mathbf{p}}{m} - \frac{e}{mc}\mathbf{A}\right) \\ &\equiv \mathbf{J}_1 + \mathbf{J}_2 \end{aligned} \tag{3.1}$$

The second of the two terms in the current,

$$\mathbf{J}_2 = -\frac{ne^2}{mc}\mathbf{A}, \tag{3.2}$$

represents the diamagnetic response of the superconducting electrons, which oppose the field. This term represents a perfect diamagnetic response. Since n is the total density of electrons, this term is independent of temperature in the superconducting state. Evidently the remaining term must cancel this diamagnetic response in order to give the correct temperature dependence of the response. For this reason $\mathbf{J}_1$ is often referred to as the *paramagnetic response*, because it

opposes the diamagnetic current. This term is also sometimes called the *quasiparticle back flow* term because it represents the flow of quasiparticles in opposition to this diamagnetic flow. However, it is important to realize that the supercurrent is actually the sum of both responses, and not just $\mathbf{J}_2$.

Let us examine the form taken by the Fourier transform of the current response. We can write the current as $\mathbf{J}(\mathbf{q}) = -(c/4\pi)K(\mathbf{q})\mathbf{a}(\mathbf{q})$, where $\mathbf{a}(\mathbf{q})$ is the Fourier transform of the field $\mathbf{A}(\mathbf{r})$. In terms of $\mathbf{J}_1$ and $\mathbf{J}_2$ we would write

$$\mathbf{J}(\mathbf{q}) = \mathbf{J}_2 + \mathbf{J}_1 = -\frac{c}{4\pi}\left[K_2(\mathbf{q}) + K_1(\mathbf{q})\right]\mathbf{a}(\mathbf{q}). \tag{3.3}$$

Now, putting in the expression for $\mathbf{J}_2$ from above and making explicit the temperature dependence of $\mathbf{J}$, we find

$$\mathbf{J}(\mathbf{q},T) = -\frac{c}{4\pi}\left[-\frac{4\pi}{c}\frac{ne^2}{mc} + K_1(\mathbf{q},T)\right]\mathbf{a}(\mathbf{q}), \tag{3.4}$$

where we can recognize the form of the first term as the London penetration depth at zero temperature, $\lambda_L^{-2}(0) = 4\pi ne^2/mc^2$. So the $K(\mathbf{q},T)$ becomes

$$K(\mathbf{q},T) = \lambda_L^{-2}(0)\left[1 + \lambda_L^2(0)K_1(\mathbf{q},T)\right]. \tag{3.5}$$

We identify the $\mathbf{q} \to 0$ limit of K as the penetration depth $K(0,T) = \lambda_L^{-2}(T)$. As mentioned earlier, we expect the (negative) K_1 term to partially cancel the temperature-independent first term, resulting in the temperature dependence of the penetration depth.

To calculate the temperature dependence of the penetration depth in the BCS model we will need to find the expression for the paramagnetic response $\mathbf{J}_1(T)$, which will give us $K_1(T)$. Recalling Eq. 3.1, we see that $\mathbf{J}_1 = ne\mathbf{p}/m$. To calculate this quantity in the BCS model we can

express the response in terms of the electron creation and annihilation operators. It can be shown that the expression is given by

$$\mathbf{J}_1(\mathbf{q}) = \frac{e\hbar}{m}\sum_{\mathbf{k}} \mathbf{k}\, c^*_{\mathbf{k}-\mathbf{q}} c_{\mathbf{k}} \tag{3.6}$$

where $\mathbf{J}_1(\mathbf{q})$ is the Fourier component of $\mathbf{J}_1$ with wave vector $\mathbf{q}$. For the purposes of the experiments described here, we will be interested in the low frequency limit, $\mathbf{q}\to 0$. In this limit the expression for $\mathbf{J}_1$ in terms of quasiparticle operators, γ, simplifies to

$$\begin{aligned}\mathbf{J}_1(0) &= \frac{e\hbar}{m}\sum_{\mathbf{k}} \mathbf{k}\left(\gamma^*_{\mathbf{k}0}\gamma_{\mathbf{k}0} - \gamma^*_{\mathbf{k}1}\gamma_{\mathbf{k}1}\right) \\ &= \frac{e\hbar}{m}\sum_{\mathbf{k}} \mathbf{k}\left(f_{\mathbf{k}0} - f_{\mathbf{k}1}\right).\end{aligned} \tag{3.7}$$

Here $f_{\mathbf{k}i}$ are the Fermi distribution functions describing the average occupation of the quasiparticle states. For small $\mathbf{a}(0)$ the occupation of the two quasiparticles states are nearly equal: $f_{\mathbf{k}0} \approx f_{\mathbf{k}1}$. The difference can be expanded to lowest order and inserted into Eq. 3.7. Using the fact that $\mathbf{J}$ is parallel to $\mathbf{a}(0)$ by symmetry, averaging $\mathbf{k}$ over the Fermi sphere to get $k_F/3$, and substituting $N(0) = 3n/4E_F$ and once again for $\lambda_L(0)$, we can show that

$$K_1(0,T) = -\left(\frac{1}{\lambda_L^2(0)}\right)\left(\frac{1}{N(0)}\right)\sum_{\mathbf{k}}\left(-\frac{\partial f}{\partial E_{\mathbf{k}}}\right). \tag{3.8}$$

Here $E_{\mathbf{k}}^2 = \xi_{\mathbf{k}}^2 + \left|\Delta_{\mathbf{k}}\right|^2$ is the quasiparticle excitation spectrum, where ξ_k is the energy relative to the Fermi energy. So to convert the sum over $\mathbf{k}$ to an integral over quasiparticle energies we must put in the density of states (DOS) of the quasiparticles, which for an ordinary *s*-wave superconductor is given by

$$\frac{N_s(E)}{N(0)} = \begin{cases} \dfrac{E}{\sqrt{E^2-\Delta^2}} & (E>\Delta) \\ 0 & (E<\Delta) \end{cases} \tag{3.9}$$

Finally, we arrive at the expression for K(0, T), giving the temperature dependence of λ_L^{-2} as

$$\lambda_L^{-2}(T) = K(0,T) = \lambda_L^{-2}(0)\left[1 - 2\int_{\Delta}^{\infty}\left(-\frac{\partial f}{\partial E}\right)\frac{E}{\sqrt{E^2-\Delta^2}}\,dE\right]. \tag{3.10}$$

For a superconductor in the local limit, at low temperature, this expression can be shown[2] to depend on temperature as

$$\frac{\lambda(T)-\lambda(0)}{\lambda(0)} \cong \sqrt{\frac{\pi\Delta(0)}{2k_BT}}\exp(-\Delta(0)/k_BT)\,. \tag{3.11}$$

We see that at the lowest temperatures the penetration depth goes as an exponential $\exp(-\Delta(0)/k_BT)$. In the nonlocal limit the temperature dependence is

$$\frac{\lambda(T)}{\lambda(0)} = \left[\frac{\Delta(T)}{\Delta(0)}\tanh\Delta(T)/2k_BT\right]^{-1/3}, \tag{3.12}$$

which is also exponential at low *T*. Qualitatively, this exponential behavior is simply the thermal excitation of quasiparticles over the energy gap. In many of the unconventional superconductors, it is believed that the energy gap goes to zero at points or lines on the Fermi surface. It is immediately obvious that the low temperature behavior in such a case must be different. As we shall see in the next section, the nodes in the energy gap give rise to power law behavior at low temperature rather than exponential as a result of the increase in the density of available quasiparticle states at low (zero) energy.

Before moving on to discuss unconventional superconductors, it is worth pointing out that the low temperature exponential behavior discussed here for the penetration depth makes itself felt more generally in any quantity which depends on the quasiparticle DOS, for example in the specific heat, ultrasound attenuation, and nuclear spin depolarization rate. Likewise, these quantities will all display power law behavior in the event that the energy gap has nodes.

3.2 Unconventional Superconductors

In this section we would like to understand how to calculate the temperature dependence of the penetration depth in unconventional superconductors. First let us take a moment to define just what is usually meant by the term *unconventional superconductor*. The *order parameter* (OP) is a quantity which is zero in the normal state and non-zero in the superconducting state. In addition, the magnitude of the OP tells us the strength of the superconducting order. A superconductor is considered unconventional if its OP has a lower symmetry than the crystal lattice of the material. The energy gap of an ordinary superconductor fits the criteria to be used as an OP. It is believed that the reduced symmetry which applies to the OP in an unconventional superconductor applies also to the energy gap. And so the energy gap can be taken as virtually synonymous with the OP.

Why is unconventional symmetry important? Consider a conventional superconductor, where the mechanism giving rise to superconductivity is well understood. In this case an attractive interaction between electrons with opposite momentum and spin is mediated by the crystal lattice in the form of phonons, giving rise to the familiar Cooper pairing. One property of this interaction is that it is isotropic, except for slight distortions due to the shape of the crystal lattice and Fermi surface. This symmetry is called *s*-wave because it represents a state with zero angular momentum, and for a cubic crystal has the familiar spherical shape of an atomic *s* orbital. Unconventional superconductors exhibit a variety of behaviors which are generally thought to be incompatible with conventional superconductivity. The assumption is that these differences can be explained if alternative mechanisms, other than phonons, give rise to superconductivity. In almost all unconventional superconductors these mechanisms are unknown. (The only exception which comes to mind is superfluid ^{3}He.[3])

One critical property of these alternative mechanisms is that they may exhibit a symmetry other than *s*-wave. In simple terms we can understand this to mean that the interaction between the electrons is anisotropic in a non-trivial way. The symmetry of this anisotropic interaction is necessarily reflected in the symmetry of the superconducting state. It turns out that a number of experiments (including the ones described in this thesis) are capable of probing the symmetry of the superconducting state. If the symmetry can be determined, it strongly constrains the possible mechanisms of superconductivity.

The microscopic theories of different sorts of unconventional interactions, applicable to different unconventional materials, are under study by many theorists. At the current time it is fair to say that there is no real consensus as to which of the leading candidates (if any) may be correct for a given material. Fortunately, in order to explore the symmetry of the superconducting state we do not need to make direct reference to any particular microscopic model of superconductivity. Instead we are guided by the phenomenological Ginzburg-Landau theory, and by the very powerful results of group theory.

Group theory breaks down the full symmetry of the crystal lattice into a certain number of irreducible representations, Γ, with basis functions $f_\Gamma(\mathbf{k}_F)$. The order parameter can be expanded in terms of all the possible basis functions as follows:

$$\Delta(\mathbf{k}_F) = \sum_\Gamma \eta^{(\Gamma)} f_\Gamma(\mathbf{k}_F), \tag{3.13}$$

where $\eta^{(\Gamma)}$ are expansion coefficients.[4] The actual realization of superconductivity is determined by the order parameter which minimizes the free energy. An important assumption is that the Ginzburg-Landau free energy functional can be expanded in powers of the order parameter, *i.e.* in powers of $\eta^{(\Gamma)}$. This expansion is written down and, by making suitable assumptions and by comparing with experiments, the expression for the free energy can be

minimized. The result is a determination of one irreducible representation which has a T_c higher than all the others. It is the symmetry of this representation which determines the symmetry of the order parameter. Of course, this procedure works equally well for conventional superconductors. By definition the result for conventional superconductors is always that the symmetry which minimizes the free energy is the usual *s*-wave symmetry.

There are two crucial properties which are determined solely by the symmetry of the OP: the parity and the presence of nodes. There are a finite number of distinct crystal lattice formations which can exist in the solid state of matter, all of which have inversion symmetry. As a result, all of the irreducible representations of the symmetry group of a crystal lattice will have definite parity, *i.e*. they have either even or odd symmetry under inversion. The reason this is so important is that the superconducting state is composed of pairs of electrons, which are Fermions, and must obey Fermi-Dirac statistics. In particular, the total state (including both orbital and spin components) must be antisymmetric under exchange of the two electrons. The critical point is this: The symmetry of the OP is the symmetry of the orbital part of the underlying superconducting state. Now, if the OP has even symmetry, as in the *s*-wave case, then the spin component of the superconducting state *must* be a singlet, because the antisymmetric symmetry of the singlet preserves the overall antisymmetry of the state. Likewise, if the OP has odd symmetry, then the spin state must have even symmetry. The spin symmetry is triplet in this case. However, we should be careful not to assume that there are three *degenerate* spin states. It is not necessarily the case that all three triplet spin states are degenerate in energy with respect to the interaction potential. If the triplet degeneracy is split then it is possible for only one or two of the states to be present. In any case, it is clear from this

brief discussion that a superconductor with triplet spin symmetry can show a wider variety of possible states than the simple *s*-wave case.

The second property of great importance which is determined by the symmetry of the OP is the presence of nodes. To illustrate the point, consider the atomic p_z orbital. This state has lobes pointing in the $\pm \hat{z}$ directions, and is zero everywhere in the *xy* plane. We will refer to this as a line node in the *xy* plane, as will become clear later. The location of the node plane is determined by the symmetry of the p_z state. If it didn't have a node in the *xy* plane, it simply wouldn't be a p_z state. The same is true of the symmetry of the OP. The nature of the nodes depends only on the symmetry of the OP. Because the energy gap of the superconductor is the OP, this has a profound effect on the behavior of the superconductor.

3.3 Nodes in the Energy Gap

The feature of unconventional superconductivity which plays the greatest role in determining the temperature dependence of the penetration depth in any given material is the presence of nodes in the energy gap. As a concrete example let us examine the so called E_{1g} state proposed for the heavy Fermion superconductor UPt_3 [4] which has the *k*-space dependence $\Delta(\mathbf{k}) \sim k_z(k_x + ik_y)$. The momentum vector is constrained to lie on the Fermi surface. Approximating the Fermi surface as spherical with unit radius, we can see that Δ will go to zero at two point nodes at the poles, $k_x = k_y = 0$, $k_z = \pm 1$. This gap function also has a line of nodes in the plane $k_z = 0$, at all values of k_x and k_y. The node structure can be seen in Fig. 3.1, which shows the energy gap and Fermi sphere on a polar plot in *k*-space.

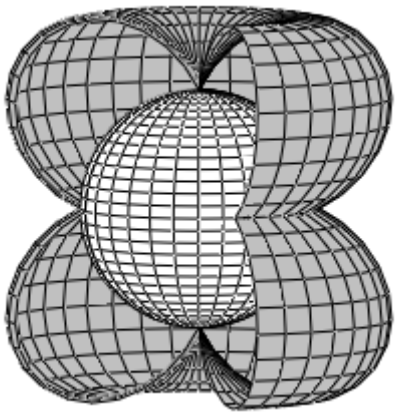

Figure 3.1
Energy gap in the E_{1g} state. The white surface is the Fermi sphere. The shaded surface is the boundary of the energy gap in *k*-space.

Annett, Goldenfeld and Renn[5] point out that the existence of nodes will depend on two factors: The symmetry of the energy gap, and the shape of the Fermi surface. For a node to exist, the gap function must vanish at a point in *k*-space where the Fermi surface exists. This is especially relevant to the case of a layered material where, rather than spherical, the Fermi surface has a cylindrical shape extending infinitely in the direction of the axis. Since the ends of the cylinder are open, this portion of *k*-space is inaccessible. Any nodes which, by symmetry consideration, would occupy this region (e.g. the point nodes in the E_{1g} state) would not, in fact, exist in this case.

Let us examine the behavior of the quasiparticle DOS when there is a node in the gap. $N(E)\,dE$ is the number of states between energy E and $E + dE$, which is proportional to the available volume of *k*-space between these energies, as illustrated in Fig. 3.2 for a point node, and Fig. 3.3 for a line node. According to Sigrist,[6] at low temperatures the form of the DOS will depend solely on the topology of the nodes. If they are line nodes, then the $N(E) \propto E$, and if they are point nodes, then $N(E) \propto E^2$.

The expression for the paramagnetic response has the form

$$K_1(0,T) \propto \int_{-\infty}^{\infty} \left(\frac{\partial f}{\partial E} \right) N_s(E)\, dE\,. \tag{3.14}$$

If $N(E) \propto E^x$

$$K_1(0,T) \propto \int_{-\infty}^{\infty} \left(\frac{\partial f}{\partial E} \right) E^x \, dE \tag{3.15}$$

To determine the temperature dependence of this expression at low temperatures, we can make the substitution $u = E / k_B T$:

$$\begin{aligned} K_1(0,T) &\propto \int_{-\infty}^{\infty} \left(\frac{\partial f}{\partial u} \right) \frac{1}{k_B T} (k_B T\, u)^x (k_B T\, du) \\ &\propto T^x \end{aligned} \tag{3.16}$$

Putting this result into Eq. 3.10 we find the low temperature limit for a point node is

$$\frac{\lambda(T) - \lambda(0)}{\lambda(0)} = \frac{\Delta\lambda(T)}{\lambda(0)} \propto T^2 \quad \text{(point node)}. \tag{3.17}$$

For the case of a line node we get the result

$$\frac{\Delta\lambda(T)}{\lambda(0)} \propto T \quad \text{(line node)}. \tag{3.18}$$

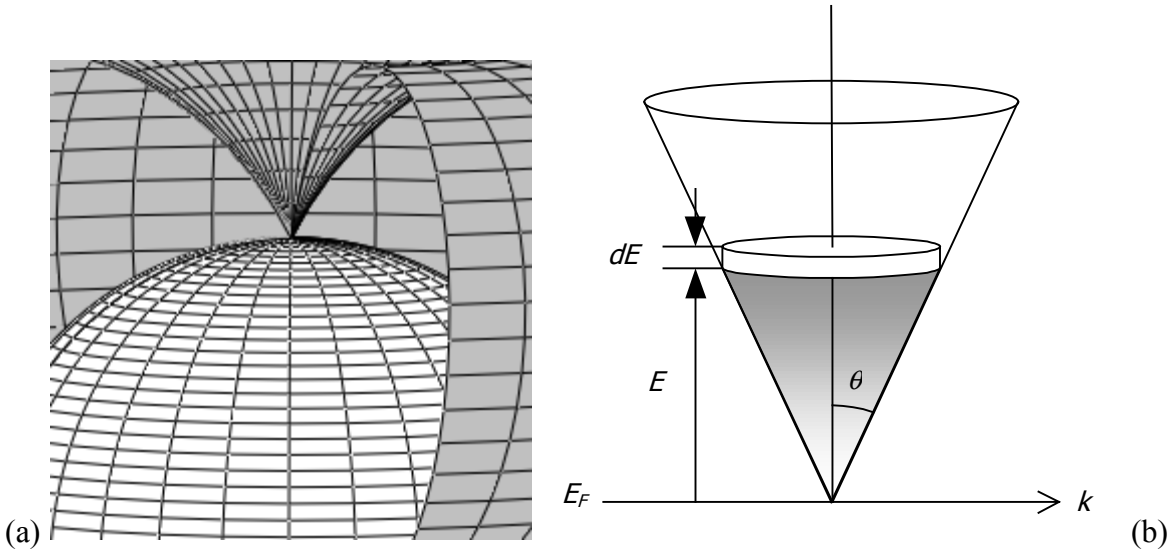

Figure 3.2

A point node in the energy gap. (a) Cutaway view of the point node of the E_{1g} state. (b) Schematic of the DOS.

So first, the observation of power law behavior in the $\Delta\lambda(T)$ is strong evidence of unconventional superconductivity, with nodes in the energy gap. And the specific power law can distinguish the dimensionality of the node structure.

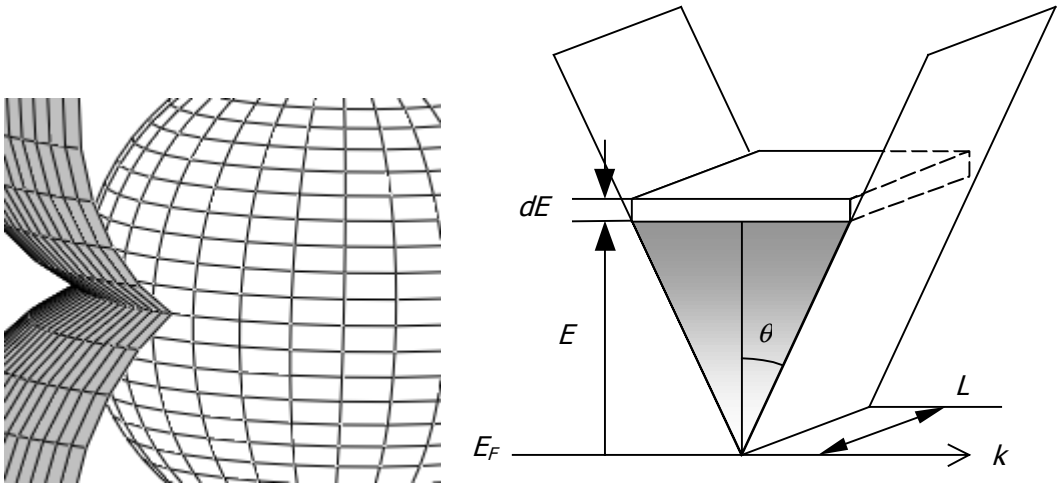

Figure 3.3

A line node in the energy gap. (a) Cutaway view of the line node of the E_{1g} state. (b) Schematic of the DOS.

The cuprate high temperature superconductors provide us with a prototype with which to compare the results of this section. In recent years, with the availability of very high quality samples of a number of these materials, $\lambda(T)$ has been found to agree very well with a model consisting of an energy gap with line nodes. However, for many years there was considerable confusion.

It is now believed that the energy gap in the cuprates has *d*-wave symmetry. These materials have a highly layered structure, with a strongly two dimensional band structure. The Fermi surface is roughly cylindrical, rather than spherical, and extends infinitely in the direction perpendicular to the planes. The energy gap is thought to have the form $\Delta(\mathbf{k}) = k_x^2 - k_y^2$. Within the planes there are nodes in the gap wherever $k_x^2 = k_y^2$, i.e. at $\pm 45°$ and

±135°, as shown in Fig. 3.4. These zeros actually constitute line nodes, since the Fermi surface extends infinitely in the k_z direction.

The early results of measurements of the $\lambda(T)$ showed clear power law behavior at low temperatures. However, rather than linear temperature dependence, as expected for line nodes, early measurements[7] showed quadratic temperature dependence. Since there was a great deal of evidence in support of the *d*-wave symmetry model, it became important to explain why this measurement appeared to be in contradiction. The idea most often cited is the presence of so-called *resonant impurity scattering* in the materials. I will discuss this idea in more detail in the next section. With this in mind, experiments were repeated with cleaner and cleaner samples as they became available. Eventually, careful measurements of very clean single crystal samples began to show that the intrinsic low temperature behavior is indeed linear in temperature, as expected for line nodes[8-12].

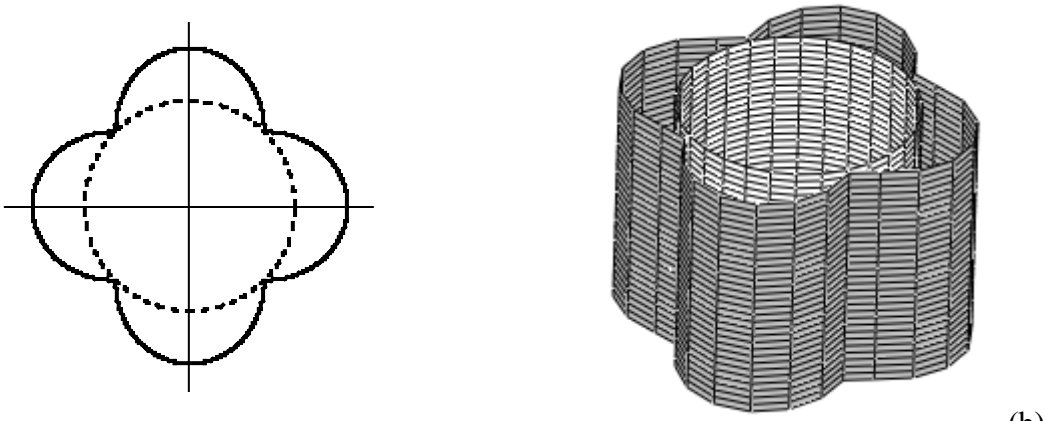

(a) (b)

Figure 3.4

The *d*-wave energy gap for the cuprate superconductors. Two dimensional picture is shown in (a) and the 3D representation in (b). Note the cylindrical Fermi surface.

3.4 Perturbing Effects

As mentioned above, the early data on $\lambda(T)$ for the curates showed quadratic temperature dependence, in contrast to the prediction of linear dependence for *d*-wave symmetry. The explanation which gained the most acceptance was the idea that resonant impurity scattering was present in the material. Another interesting idea is the proposal that, despite the fact that the coherence length is usually thought to be much shorter than the penetration depth, the presence of nodes in the gap necessitates a nonlocal treatment of the calculation.

3.4.1 Resonant Impurity scattering

The hypothesis of resonant impurity scattering (RIS), also called unitary scattering, was proposed by Hirschfeld and Goldenfeld[13] to explain a number of behaviors observed in measurements of the cuprate YBCO. Most important is the discrepancy already mentioned: that some measurements showed quadratic temperature dependence, while other, equally credible measurements showed linear behavior. The critical temperatures in all these cases were at or near the optimal values attained for these materials. This argues against the possibility of weak Born scattering, which would tend to strongly suppress T_c. In addition, measurements of thermal conductivity and specific heat had been reported which seemed to be consistent with resonant impurity scattering.

Hirschfeld and Goldenfeld made several predictions based on the RIS hypothesis. They predicted the existence of a cross-over temperature T^*. Above T^* the intrinsic behavior is seen: $\Delta\lambda(T) \sim T$. But at lower temperature RIS causes the behavior to become $\Delta\lambda(T) \sim T^2$. An important point is that in the strong scattering limit small concentrations of impurities can cause a large residual DOS at low temperature, without significantly suppressing T_c. For example, if the resonant defect concentration is 1%, they calculate T^* about 10% of T_c. Meanwhile, T_c

would be suppressed by only 1%. At more realistic concentrations of only 0.1%, T^* would be as low as 2-3% of T_c. No explanation is given, however, for the source of RIS.

The predictions quoted here are very interesting. They suggest that if we can make measurements down to sufficiently low temperature, it should be possible to observe the crossover of a linear sample to quadratic behavior, verifying the RIS model.

3.4.2 Nonlocal Effects

A different idea has been proposed by Kosztin and Leggett[14] to explain the quadratic dependence. They point out that calculations have been made in the cuprates assuming the local limit. This seems reasonable at first glance since average coherence lengths are on the order of several Ångstroms, which is small compared to the penetration depths of several thousand Ångstroms. However, the coherence length, can be expressed as $\xi_0 = v_F / \pi\Delta_0$. Considering that $\Delta_0 = \Delta_0(\mathbf{k})$ is anisotropic, it might be more appropriate to adopt an anisotropic coherence length, $\xi(\mathbf{k}) = v_F / \pi\Delta(\mathbf{k})$. Under this assumption, the coherence length can be seen to diverge at points on the Fermi surface where the gap vanishes. In these directions nonlocal effects could be important. Nonlocal electrodynamics would be expected to be important on only a small fraction of the Fermi surface, of order $a_0 \equiv \xi_0 / \lambda_0$. The absolute value, $\lambda(0)$, would not be significantly affected because the whole Fermi surface contributes to its value. However, the low temperature power law could be strongly affected because the effect is concentrated around the nodes of the gap, which, as we have seen, dominate the temperature dependence.

This paper predicts a crossover temperature (in units where $k_B = 1$), $T^* = \alpha_0\Delta_0 = \xi_0\Delta_0 / \lambda_0$, below which these effects will be important. For YBCO, with typical values $\Delta_0 \approx$ 250 K, $\xi_0 \approx$ 14 Å, and $\lambda_0 \approx$ 1400 Å, we find $T^* \approx$ 25 K. An important result of this

calculation for YBCO is that the nonlocal effects will not be seen for magnetic fields parallel to the *ab* planes. This occurs because the wavevectors for the quasi-two dimensional YBCO are constrained to lie in the *ab* plane, and will not have a component parallel to direction of field penetration (the *c* direction) in this orientation. Finally, the conclusion is the same as the previous section: at low temperature, but above T^*, linear behavior will be observed, while below T^* the behavior will cross over to quadratic.

It is interesting to consider this scenario for the material Sr_2RuO_4, under study in this thesis. Putting in typical measured values of penetration depth, coherence length and energy gap, we find a value $T^* \approx T_c$. This will be discussed further in the chapter on Sr_2RuO_4.

References

1 M. Tinkham, *Introduction to Superconductivity* (McGraw-Hill, Inc., New York, 1996).

2 B. Muhlschlegel, Zeitschrift fur Physik **155**, 21 (1959).

3 A. Leggett, Reviews of Modern Physics **47**, 331 (1975).

4 J. A. Sauls, Advances in Physics **43**, 113 (1994).

5 J. Annett, N. Goldenfeld, and S. R. Renn, in *Physical Properties of High Temperature Superconductors*, edited by D. M. Ginsberg (World Scientific, Singapore, 1990), Vol. 2.

6 M. Sigrist and K. Ueda, Reviews of Modern Physics **63**, 239 (1991).

7 J. Annett, N. Goldenfeld, and S. R. Renn, Physical Review B **43**, 2778 (1991).

8 S.-F. Lee, D. C. Morgan, R. J. Ormeno, *et al*., Physical Review Letters **77**, 735 (1996).

9 D. M. Broun, D. C. Morgan, R. J. Ormeno, *et al*., Physica C **282**, 1467 (1997).

10 W. N. Hardy, D. A. Bonn, D. C. Morgan, *et al*., Physical Review Letters **70**, 3999 (1993).

11 K. Zhang, D. A. Bonn, S. Kamal, *et al*., Physical Review Letters **73**, 2484 (1994).

12 O. Waldmann, F. Steinmeyer, P. Muller, *et al*., Physical Review B **53**, 11825 (1996).

13 P. Hirschfeld, J. and N. Goldenfeld, Physical Review B **48**, 4219 (1993).

14 I. Kosztin and A. Leggett, Physical Review Letters **79**, 135 (1997).

4 Strontium Ruthenate

Strontium ruthenate (SRO) is the first reported perovskite superconductor without copper. With a chemical formula Sr_2RuO_4, it has the same crystal structure as the high temperature superconductor La_2CuO_4. While SRO has been known for some time,[1] it was not until more recently that SRO was shown to be a superconductor.[2] Critical temperatures of the earliest samples were around 1 K, with more recent samples displaying T_c as high as 1.5 K.

As superconductivity in SRO was investigated in detail, it quickly became apparent that SRO is an unconventional superconductor. The experimental evidence, when taken together with theoretical models, seems to support the conclusion that SRO has *p*-wave symmetry.

I will discuss the experimental measurements that have been made on SRO, and review the important features of the theories which have been proposed to explain the unconventional nature of superconductivity in this material.

4.1 Crystal Growth and Characterization

The first report of superconductivity in SRO came from Maeno *et al*.[2]. High quality crystals are grown using a floating zone method in air or in a controlled atmosphere of 10% oxygen and 90% argon using excess Ru as a flux. It was found that a mixture of SRO and pure Ru metal forms a eutectic. This results in a characteristic spontaneous separation of the two components of the eutectic. The result is that Sr_2RuO_4 crystallizes in its exact stoichiometry from a mixture containing excess Ru, with pockets of pure Ru metal forming a lamellar structure embedded in a single crystal Sr_2RuO_4 matrix.[3] Maeno *et al*. found that a radial concentration gradient of Ru forms in the cross section of the growth rod. The outer surface has a lower concentration of Ru, and in a sheath approximately 0.5 mm thick, pure Sr_2RuO_4

crystallizes. It is from this region that samples of pure SRO are taken. The eutectic matrix of SRO and Ru forms in the remaining core of the rod. Material from this region has shown some unusual behavior, including an apparent enhancement of T_c to about 3 K. This is above that of pure SRO (1.5 K) and far above that of pure Ru (0.5 K).

The powder x-ray diffraction spectra of pure SRO shows a body-centered tetragonal lattice with the perovskite structure of K_2NiF_4, and is isostructural to the high temperature superconductor La_2CuO_4. Lattice parameters were found to be as follows: $a = b = 0.387$ nm and $c = 1.274$ nm at room temperature.[2]

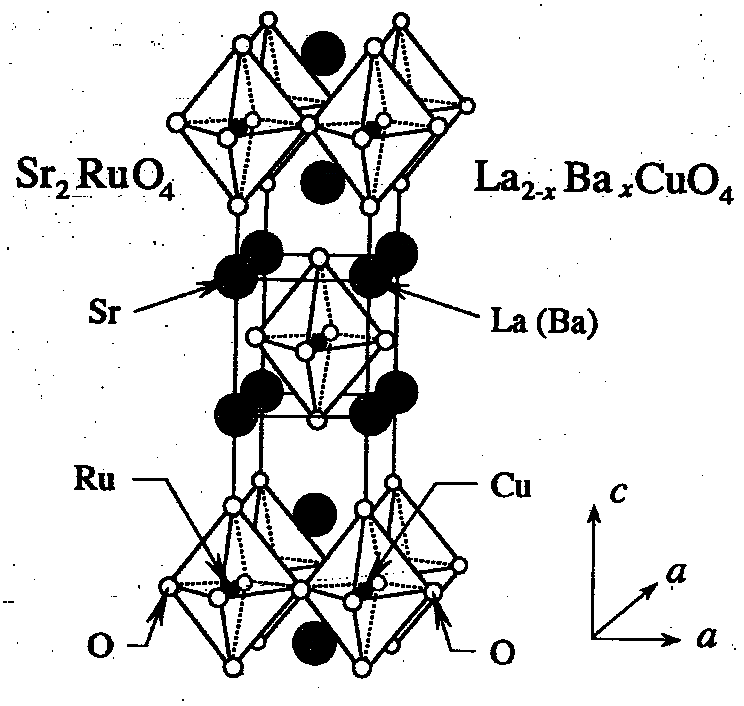

Figure 4.1
Crystal structure of Sr_2RuO_4 and $La_{2-x}Ba_xCuO_4$ from Maeno.[2]

The band structure of SRO has been subject to some controversy thanks to the possibility of measuring the Fermi surface by two different techniques. Measurements of angle resolved photo-emission spectroscopy (ARPES) were the first to probe the Fermi surface, which was followed a short time later by measurements based on the de Haas-van Alphen (dHvA) and Shubnikhov-de Haas (SdH) effects. The dHvA and SdH results disagree with the

ARPES in a rather important way. The best evidence now suggests that the dHvA and SdH data are most likely correct.

ARPES measurements were made by Yokoya *et al*.[4] They found three Fermi surface sheets: one electron-like sheet (labeled α) centered at the Γ point of the Brillouin zone and two hole-like sheets (β and γ) centered at the *X* point. This disagrees with band structure calculations[3, 5] which predict two electron-like sheets centered at the Γ point and one hole-like sheet centered at the *X* point. In addition, Yokoya *et al*. reported the possibility of an extended van Hove singularity. The ARPES electron count agrees with the band structure calculations. But later measurements by Puchkov *et al*.[6] cast doubt on the van Hove singularity.

Mackenzie *et al*.[7, 8] measured the Fermi surface by observing quantum oscillations of magnetization (dHvA effect) and resistivity (SdH effect). Their results agree with the calculated band structure: α sheet hole-like, β and γ sheets electron-like. The γ sheet closes around the Γ point instead of the *X* point.

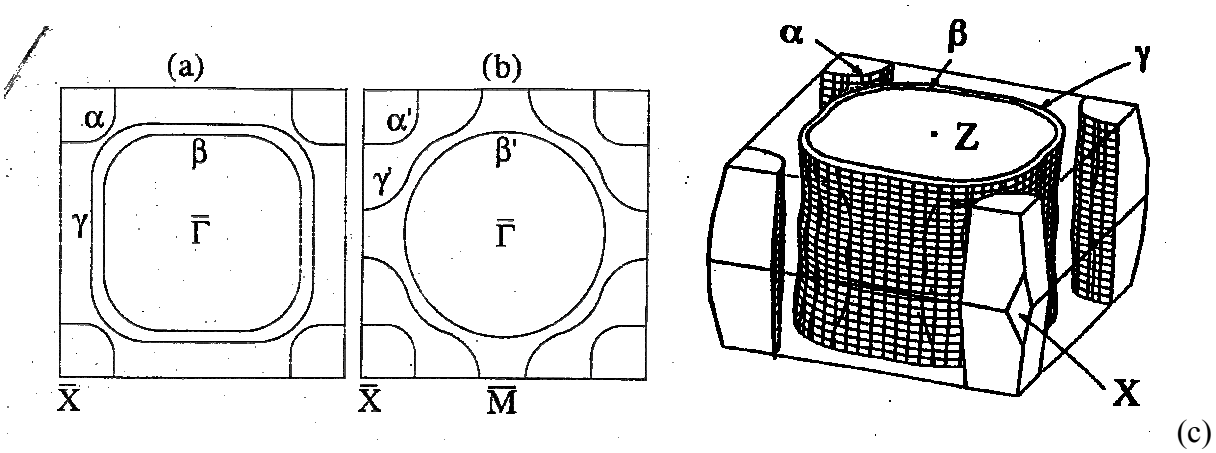

Figure 4.2

Fermi surface of SRO. (a) Schematic dHvA effect result and (b) ARPES result (both from Mackenzie[8]) (c) Result expected from band structure calculations (from Maeno[9], after Mackenzie[7])

The controversy has largely been resolved in favor of the dHvA results. ARPES measures only the surface of the sample, whereas dHvA effect measures the bulk material. It is likely that the ARPES data is not representative of the bulk due to a rearrangement of the bonds at the surface of freshly cleaved samples, which distorts the Fermi surface locally.

It is interesting to note that dHvA measurements have not been made on the high temperature superconductors. This experiment is only possible at very low temperatures, in very pure samples, and requires a magnetic field which exceeds H_{c2}, so that the field penetrates the material uniformly. The HTSC materials can be divided into two categories: those which require doping to be superconducting, and those which are superconducting at stoichiometric concentrations. Some which require substitutional doping, such as $La_{2-x}Sr_xCuO_4$, have values of H_{c2} which can be reached in the laboratory, but the random nature of doping makes dHvA effect unobservable. The stoichiometric materials, such as $YBa_2Cu_3O_7$, have high values of H_{c2} currently unattainable in the laboratory (at least for non-pulsed magnets required for dHvA measurements). Akima *et al.*[10] measured H_{c2} for SRO for fields applied parallel to the *ab* plane and parallel to the *c*-axis, finding $\mu_0 H_{c2,ab}(0) = 1.5$ T and $\mu_0 H_{c2,c}(0) = 0.075$ T. The relatively low values of H_{c2} provides a unique opportunity to measure the Fermi surface of a perovskite superconductor with both ARPES and dHvA effects.

Below 25 K the resistivity shows SRO to be a two dimensional Fermi liquid, with $\rho(T) = \rho(0) + AT^2$ behavior indicating the importance of electron-electron scattering at low temperatures. The resistivity is anisotropic, with residual low *T* values of $\rho_{ab}(0) = 0.9$ μΩcm and $\rho_c(0) = 500$ μΩcm.[9]

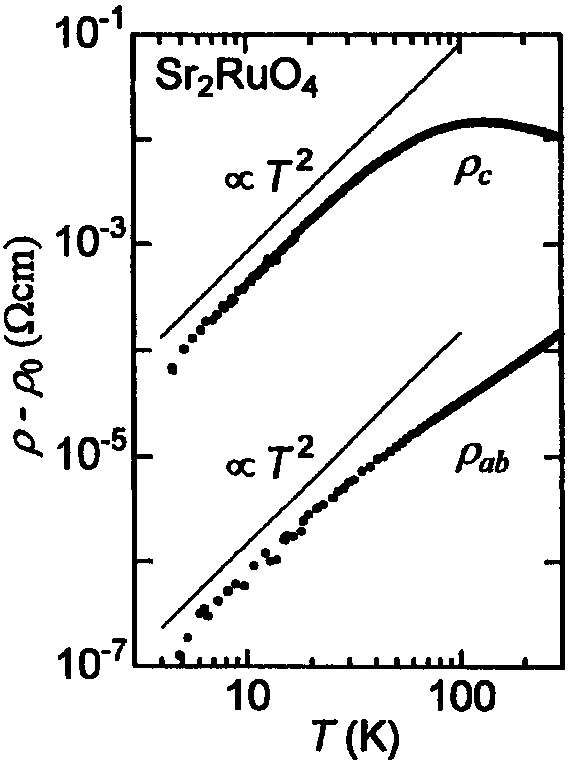

Figure 4.3

Resistivity of SRO from Maeno.[9]

4.2 Superconducting Properties

A large number of different measurements have been made of the superconducting properties of SRO. On the whole they paint a consistent picture of SRO as an unconventional superconductor. Important results have been reported from measurements of muon spin relaxation (μSR), from nuclear magnetic resonance (NMR) and nuclear quadrupole resonance (NQR) measurements of nuclear spin relaxation time and electronic spin susceptibility, from specific heat and thermal conductivity, and from studies of the effect of impurities and disorder on the superconducting properties. I will review these results and discuss their relevance to issues of unconventional superconductivity in SRO.

The most pivotal evidence for unconventional superconductivity is the ^{17}O nuclear quadrupole resonance (NQR) measurement of the temperature dependence of the Knight shift. The measurement shows that there is no change in the spin susceptibility of the electrons, for

magnetic fields parallel to the crystal planes, as the sample enters the superconducting state.[11] In contrast, in a conventional superconductor, the pairing of electrons with opposite spin in the superconducting state causes an abrupt drop in the spin susceptibility. The absence of this effect in SRO suggests strongly that this material has spin-triplet pairing. In the so-called "equal-spin pairing" triplet state electrons form pairs where both have the same spin. That is to say, the electrons are paired as $(k\uparrow, -k\uparrow)$ and $(k\downarrow, -k\downarrow)$. In this case the electrons retain the same polarizability as in the normal state, and hence there is no change in the spin susceptibility in the superconducting state.[12]

The total wavefunction for a fermion system must have odd parity. If SRO has triplet spin parity (even) this implies that its orbital part (and the order parameter) must have odd parity, and thus cannot be *s*-wave. If one believes the Knight shift data to be correct, this is convincing evidence that SRO is not only an unconventional superconductor, but that it must have odd parity. It is irresistible to draw a correspondence between the superconductor SRO and the superfluid ^{3}He, which was also shown to have spin-triplet pairing.[12]

A second experiment with important implications on the pairing state is muon spin-relaxation (μSR) measurements. Spin-polarized muons are fired into the material where they come to rest for a short time before decaying. Positrons are emitted preferentially along the direction of the spin, allowing the detection of the average polarization at the time of decay. In the presence of a magnetic field the spin of each muon will precess. So the relaxation of the polarization measures the local magnetic field inside the material. In the absence of magnetic order, the interaction of the muons with the randomly oriented nuclear spins relaxes the polarization at a characteristic rate. The appearance of a magnetic field or internal magnetic ordering can then be detected as an additional relaxation rate on top of this background.

Measurements of μSR by Luke *et al*.[13] on SRO show an increase in the relaxation rate below T_c. This seems to indicate that below T_c a magnetic field is spontaneously generated in the bulk material of SRO in the superconducting state. This field is apparently spatially non-uniform, and static on the microsecond time scale. The presence of spontaneous magnetic fields, or equivalently spontaneous current, is a signature of time-reversal symmetry-breaking. Luke *et al*. suggest that the broad distribution of field sources evident within SRO might be associated with variations of the order parameter around dilute impurity sites or domain walls. We are again reminded of ^{3}He where it is thought the superfluid A phase breaks time-reversal symmetry.[12] Another unconventional superconductor showing similar behavior is the heavy-fermion superconductor UPt_3, which is believed to have unconventional symmetry, and which also shows the appearance of spontaneous magnetization below T_c.[14]

Two very important results have come from NMR and NQR measurements on SRO. The first is the measurement of the Knight shift, which I have already mentioned. The second, measurements of nuclear spin lattice relaxation rate, $1/T_1$, showed the absence of the usual Hebel-Slichter enhancement just below T_c, and power law behavior at low temperatures.[15] Recent results have shown $1/T_1 \propto T^3$, consistent with an OP with line nodes.[16]

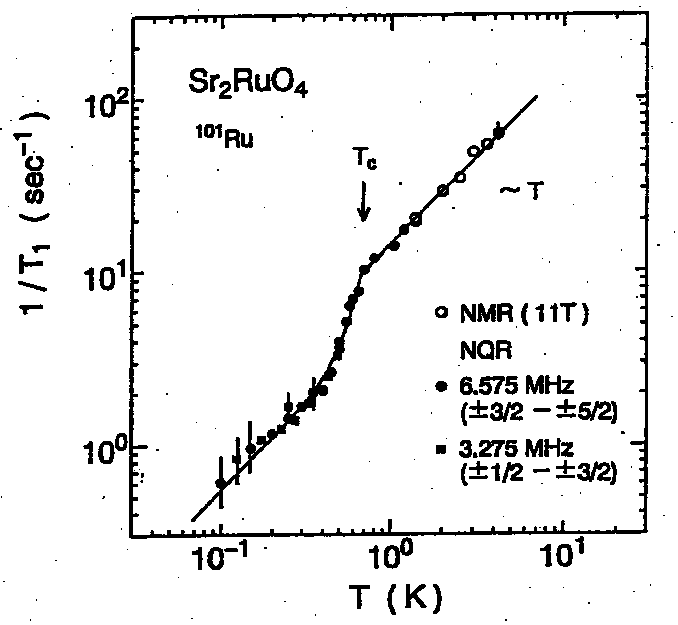

Figure 4.4
Nuclear spin relaxation rate of SRO from Ishida[15]

The T_c of SRO was shown to be extremely sensitive to non-magnetic impurities.[17] Whereas ordinary *s*-wave superconductors are sensitive to magnetic impurities, their critical temperatures are relatively insensitive to non-magnetic impurities. In contrast, unconventional superconductivity can be strongly suppressed by *non*-magnetic impurities. For example, this effect has been seen in UPt_3.[18]

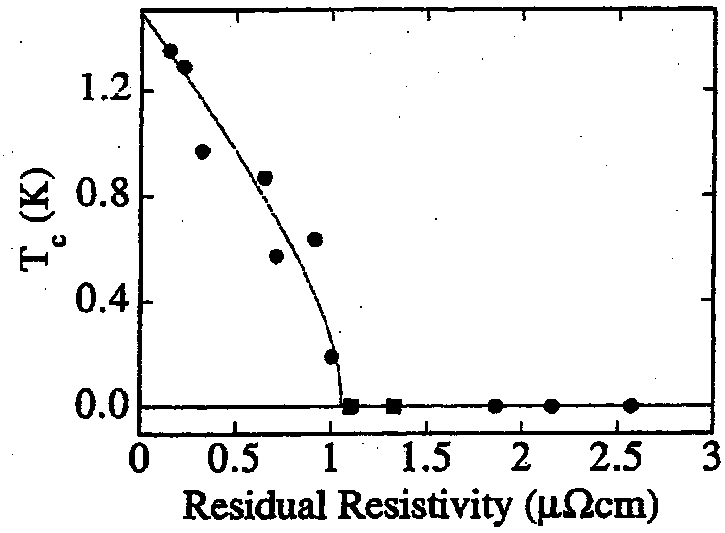

Figure 4.5
Suppression of critical temperature of SRO by impurities from Mackenzie.[17] Residual resistivity is inversely proportional to the zero temperature mean free path.

The thermal conductivity at low temperatures is one property which depends upon the quasiparticle excitation spectrum of the superconductor. Ordinary superconductors show a strongly reduced thermal conductivity when the temperature drops below the level where thermal energy can excite quasiparticles over the superconducting energy gap. At low temperatures $\kappa \sim \exp(-\Delta / k_B T)$. In early measurements on SRO, κ was found to follow a power law behavior $\kappa \sim aT + bT^2$ suggesting that SRO could be an unconventional superconductor.[19] In addition the thermal conductivity remained unusually high as T approached zero, indicating the presence of a residual density of states (DOS). The authors used samples with T_c less than 1 K, and acknowledge that the relatively high content of non-magnetic impurities is at least partly responsible for the residual DOS. As I mentioned in regard to the suppression of T_c, in an unconventional superconductor non-magnetic impurities can break superconducting pairs, which would give rise to an excess DOS as observed here. So this can be taken as evidence for unconventional superconductivity.

Another measurement which also shows a residual DOS at low temperatures is the specific heat. Nishizaki *et al*.[20] measured samples with T_c ranging from 0.7 to 1.2 K. They found that as T_c increases, the value of γ_S / γ_N appeared to approach 1/2, where γ_N and γ_S are the coefficients of the linear term in the specific heat in the normal state and in the superconducting state, respectively, as T approaches zero. In an ordinary superconductor γ_S would be expected to approach zero in the low temperature limit with an exponential temperature dependence. The rather high value is again suggestive that a residual DOS exists at low temperature. Once again impurity scattering can be important in analyzing this result. The authors argue that their data are most consistent with an anisotropic energy gap containing line nodes.

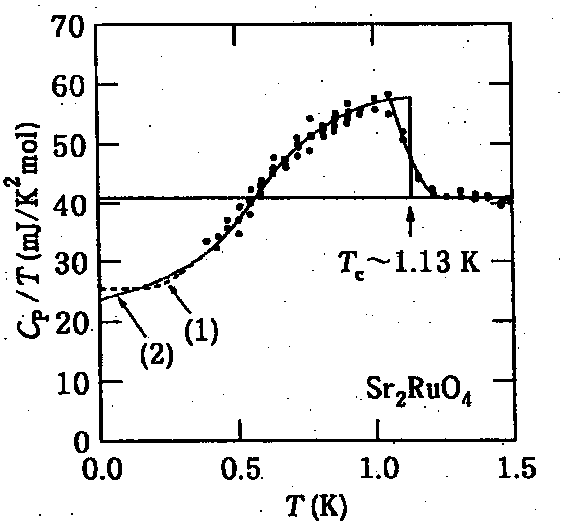

Figure 4.6

Specific heat of SRO from Maeno[9]

Some theorists have incorporated the residual DOS seen in thermal conductivity and specific heat as an important feature to be explained by their models. I will discuss the details of these models in the next section. However, I would like briefly to mention that this point of the theories may be in error. In both of these cases the samples have at least a moderate level of impurities which, as I explained, can give an increased DOS. Data on the specific heat have recently become available on higher quality samples, down to lower a temperature of 0.1 K.[21] Their results show that C/T continues to drop at the same rate as previously measured, with no crossover or transition evident. This data reduces the upper limit of γ_S / γ_N from ~1/2 to ~0.35. This data also displays a clear linear temperature dependence of C/T, consistent with line nodes in the energy gap.

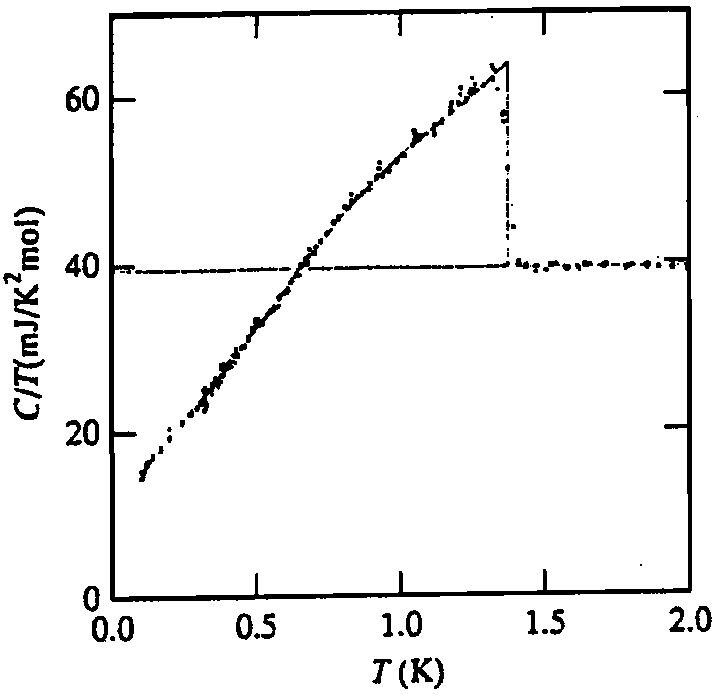

Figure 4.7
New specific heat data from Maeno[21]

Akima *et al.*[10] used their measurements of H_{c2}, mentioned in the previous section, to calculate the anisotropic coherence lengths, ξ_{ab} and ξ_c, in terms of the upper critical fields and the magnetic flux quantum, Φ_0, using the Ginzburg-Landau formulas for an anisotropic superconductor, $H_{c2\|c} = \Phi_0/(2\pi\xi_{ab}^2)$, and $H_{c2\|ab} = \Phi_0/(2\pi\xi_{ab}\xi_c)$. They find the zero temperature values $\xi_{ab}(0) = 660$ Å and $\xi_c(0) = 33$ Å. We can compare these values with the small angle neutron scattering estimate of the zero temperature penetration depth by Riseman *et al.*,[22] who find $\lambda_{ab}(100\text{ mK}) = 1940 \pm 160$ Å. The cuprates are firmly placed in the local limit since their penetration depth is several orders of magnitude larger than their coherence length. However, in SRO at low temperatures we see that the coherence length and penetration depth are different by only a factor of three. SRO is clearly *not* in the extreme local limit and, even based on these values alone, should probably be considered marginally nonlocal. In the next chapter I will argue that, on the basis of our results indicating the possible presence of nodes in the energy gap, SRO should be considered a nonlocal unconventional superconductor.

Finally, there is some recent evidence for unusual behavior of vortices at low temperatures. Mota *et al*.[23] have reported on measurements of magnetic flux flow. They cool the sample in a magnetic field and observe the rate at which magnetic flux escapes under the influence of the mutual repulsion of the vortices and the pinning in the material. They find that at ~50 mK there is an abrupt drop in the flux creep. They attribute this result in SRO to a second superconducting transition from a state which does not break time reversal symmetry into one that does. They base this conclusion on their observation of a nearly identical effect in UPt_3 at the lower of its two superconducting transitions, where it is believed to break time reversal symmetry.[24] Mota *et al*. suggest that in the time reversal symmetry breaking state, vortices become strongly pinned at the boundaries between domains of alternating (broken) time reversal symmetry. It is not clear how this result should be reconciled with the μSR measurement which shows that time reversal symmetry is broken not at 50 mK, but right at T_c. It might be possible to detect this sudden breaking of time reversal symmetry using our tunnel diode oscillator system if the sample were cooled in an applied magnetic field, rather than zero-field cooled as it is for the results reported in this thesis.

Measurements of the temperature dependence of the penetration depth can play an important role in resolving some of the questions about SRO which remain unanswered. As discussed in chapter 3 the penetration depth at low temperatures is sensitive to the DOS. Observation of power law behavior in penetration at low T is indicative of nodes in the energy gap.

4.3 Prominent Theoretical Concepts

Any theory to explain superconductivity in SRO must account for the results described in the previous section. The most important being the following: triplet spin-symmetry, spontaneous time-reversal symmetry breaking, and residual DOS at low temperature.

There are two different models which have been proposed, which have attracted significant attention. They each explain the residual DOS in a fundamentally different way. The first is based on a non-unitary order parameter (OP) which can be shown to give rise to an excitation spectrum which is gapped for half of the electronic system, and gapless for the other half. The second is based on so called *orbital dependent superconductivity* (ODS), which posits that only one of the three Fermi surface sheets is superconducting, the remaining two sheets then providing the excess DOS.

4.3.1 Non-Unitary Model

The non-unitary model has been proposed by Machida *et al*.[25] and independently, in a similar formulation, by Sigrist and Zhiromirsky.[26] In a triplet superconductor, a compact notation is used to represent the spin and orbital parts of the OP, $\Delta(k)$, in terms of a vector **d** as follows:

$$\begin{aligned}\Delta(\mathbf{k}) &= i\mathbf{d}\cdot\boldsymbol{\sigma}\sigma_y \\ &= i\sum_{\mu} d_{\mu}(\mathbf{k})\sigma_{\mu}\sigma_y\end{aligned} \tag{4.1}$$

where σ_{μ} are the Pauli spin matrices. Writing out the components of the matrices explicitly we find

$$\Delta(\mathbf{k}) = \begin{bmatrix} -d_x + id_y & d_z \\ d_z & d_x + id_y \end{bmatrix} \tag{4.2}$$

where each of the components of **d** depends on **k**. If **d** is unitary it can be shown that the quasiparticle excitation spectrum behaves as

$$E_{\mathbf{k}} = \sqrt{\xi_{\mathbf{k}}^2 + \left|\mathbf{d}(\mathbf{k})\right|^2} \tag{4.3}$$

where $\xi_{\mathbf{k}} = \varepsilon_{\mathbf{k}} - \varepsilon_{\mathrm{F}}$ is the energy relative to the Fermi energy. In this case $\left|\mathbf{d}\right|^2$ represents the magnitude of the energy gap in the excitation spectrum. One must provide this minimum energy in order to create a quasiparticle.

If **d** is allowed to be non-unitary, the excitation spectrum generalizes to

$$E_{\mathbf{k},\pm} = \sqrt{\xi_{\mathbf{k}}^2 + \left|\mathbf{d}(\mathbf{k})\right|^2 \pm \left|\mathbf{d}^*(\mathbf{k}) \times \mathbf{d}(\mathbf{k})\right|}\,. \tag{4.4}$$

If **d** is non-unitary then $\mathbf{d}^*$ points in a different direction than **d** and the cross product is non-zero. The excitation spectrum splits into two branches for the plus and minus cases. Notice that the cross product term can be taken as a measure of the non-unitarity of the OP. When **d** is maximally non-unitary $\left|\mathbf{d}^* \times \mathbf{d}\right| = \left|\mathbf{d}\right|^2$ and the gap of the minus branch of the excitation spectrum vanishes. This is the scenario which has been proposed to explain the excess DOS in SRO in the non-unitary models.

Sigrist and Zhitomirsky propose that the OP has the form $\mathbf{d}(\mathbf{k}) = (\hat{\mathbf{x}} \pm i\hat{\mathbf{y}})(k_x \pm ik_y)$. This OP is maximally non-unitary so exactly half the excitation spectrum is gapless. It has triplet spin symmetry, *p*-wave orbital symmetry, and breaks time-reversal symmetry. The branch of the excitation spectrum which shows a gap is isotropic in *k*-space. Exactly half of the quasiparticles would be subject to this energy gap. The penetration depth $\lambda(T)$ can be expected to show exponential dependence at low temperatures, as in an *s*-wave superconductor, because the same freezing out of excitations occurs as the thermal energy drops below the gap energy. The gapless quasiparticles would not contribute significantly to the temperature dependence of

the penetration depth. Additionally, it is not clear how a state of this symmetry can be stabilized from the standpoint of free energy, as discussed in Ch. 3.

4.3.2 Orbital-Dependent Superconductivity

The orbital-dependent superconductivity (ODS) model has been proposed by Agterberg, Rice and Sigrist.[27] This model accounts for the excess DOS differently than the previous model. The argument goes as follows: The band structure in SRO is derived from three Ru *d* orbitals: d_{xy}, d_{xz}, and d_{yz}. They claim that the two dimensional nature of the electronic dispersion implies that the bands break into two classes: *xy* and $\{xz, yz\}$. The pair scattering amplitude *between* these two classes of bands will be significantly smaller than the scattering *within* each class for an unconventional OP. It is expected that the two sets of bands will essentially behave independently with regard to superconductivity. Thus it is predicted that at T_c a larger gap will form on the γ Fermi surface sheet and a smaller (if any) gap on the α and β sheets. This will create essentially gapless excitations for temperatures in excess of this smaller gap, which accounts for the excess DOS.

Sigrist *et al*. [28] propose that the OP which best accounts for the experimental data is the two-dimensional analogue of the *A* phase of superfluid ^{3}He: $\mathbf{d}(\mathbf{k}) = \hat{\mathbf{z}}(k_x \pm ik_y)$. This state has *p*-wave (triplet) symmetry and breaks time-reversal symmetry, as in the previous model, but it is unitary. The magnitude of this energy gap is isotropic in *k*-space. In the simplest case, a gap forms on the γ Fermi surface sheet, and no gap at all forms on the others. We would expect to see exponential behavior of $\lambda(T)$ once again, by the same argument as we used for the non-unitary model. However, there are several other possible scenarios.

Multi-band superconductivity has been observed only in very rare cases. One example is the study by Binnig *et al*.,[29] who observed two-band superconductivity in $SrTiO_3$ doped with

Nb, with critical temperatures less than 0.6 K. As a function of doping, free carriers fill a second conducting band. Above a critical doping level two energy gaps are observed in tunneling measurements, each with a qualitatively different temperature dependence. In this case both energy gaps become nonzero at the same temperature.

Under the ODS model there are some similar effects which might be observable. The first is the crossover in temperature dependence of properties like penetration depth, which depend on the DOS. As the temperature is reduced below the level of each energy gap activated (exponential) behavior would be observed for each gap in turn. Another possibility is that the superconductivity on the α and β sheets might actually have their own critical temperature, lower than the γ sheet. One might conceivably observe a second superconducting transition at some lower temperature. Both of these effects, if present, would be observable in our measurements of the penetration depth. However, I would like to point out that, while the possibility of observing these types of effects was an important motivation in our study of SRO, we observed no such effects in our measurements.

4.3.3 Ferromagnetic Spin Fluctuation Model

Miyake and Narikiyo[30] point out that neither the ODS model nor the non-unitary model can easily explain the absence of the Hebel-Slichter peak observed in the NMR nuclear spin relaxation rate. In their theory, they propose that short range ferromagnetic spin fluctuations give rise to triplet pairing. They write down a pairing interaction based upon interaction of electrons located at nearest neighbor sites on a square lattice. Assuming the state will break time reversal symmetry, in order to agree with the μSR measurements, Miyake and Narikiyo propose an order parameter of the form $\mathbf{d}(\mathbf{k}) = \hat{\mathbf{z}}(\sin k_x \pm i \sin k_y)$. The amplitude of this state

will vanish at any points on the Fermi surface which pass through the points $\mathbf{k} = (0, \pm\pi)$, $(\pm\pi, 0)$ and $(\pm\pi, \pm\pi)$. If the Fermi surface only pass close to these points, the OP will not vanish, but will be highly anisotropic. To parameterize the shape of the Fermi surface we can write $\mathbf{k}_F = (\pi R\cos\theta_k, \pi R\sin\theta_k)$, where *R* parameterizes the radius of the Fermi circle. The amplitude of the OP as a function of θ_k, the angle in *k*-space, is shown in Fig 4.8 for the value R = 0.9, which Miyake and Narikiyo suggest is realistic for SRO. The amplitude is quite anisotropic, and might be consistent with the same power law behavior which would be expected for an exact node line in the OP.

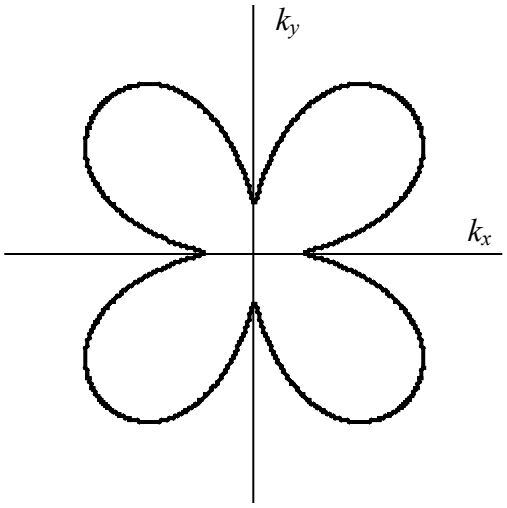

Figure 4.8
Reciprocal space polar plot in the *ab* plane of the OP for the ferromagnetic fluctuation model of Miyake and Narikiyo with Fermi surface scale factor *R* = 0.9.

References

1 J. J. Randall and R. Ward, Journal of the American Chemical Society **81**, 2629 (1959).

2 Y. Maeno, H. Hashimoto, K. Yoshida, *et al*., Nature **372**, 532 (1994).

3 Y. Maeno, T. Ando, Y. Mori, *et al*., Physical Review Letters **81**, 3765 (1998).

4 T. Yokoya, A. Chainani, T. Takahashi, *et al*., Physical Review B **54**, 13311 (1996).

5 T. Oguchi, Physical Review B **51**, 1385 (1995).

6 A. V. Puchkov, Z. X. Shen, T. Kimura, *et al*., Physical Review B **58**, 13322 (1998).

7 A. P. Mackenzie, S. R. Julian, A. J. Diver, *et al*., Physical Review Letters **76**, 3786 (1996).

8 A. P. Mackenzie, S. Ikeda, Y. Maeno, *et al*., Journal of the Physical Society of Japan **67**, 385 (1998).

9 Y. Maeno, S. Nishizaki, K. Yoshida, *et al*., Journal of Low Temperature Physics **105**, 1577 (1996).

10 T. Akima, S. NishiZaki, and Y. Maeno, Journal of the Physical Society of Japan **68**, 694 (1999).

11 K. Ishida, H. Mukuda, Y. Kitaoka, *et al*., Nature **396**, 658 (1998).

12 A. Leggett, Reviews of Modern Physics **47**, 331 (1975).

13 G. M. Luke, Y. Fudamoto, K. M. Kojika, *et al*., Nature **394**, 558 (1998).

14 G. M. Luke, A. Keren, L. P. Le, *et al*., Physical Review Letters **71**, 1466 (1993).

15 K. Ishida, Y. Kitaoka, K. Asayama, *et al*., Physical Review B **56**, 505 (1997).

16 K. Ishida, (Private communication, 1999).

17 A. P. Mackenzie, R. K. W. Haselwimmer, A. W. Tyler, *et al*., Physical Review Letters **80**, 161 (1998).

18 J. B. Kycia, J. I. Hong, M. J. Graf, *et al*., Preprint , 0 (1997).

19 H. Suderow, J. P. Brison, J. Flouquet, *et al*., Journal of Physics: Condensed matter **10**, 597 (1998).

20 S. Nishizaki, Y. Maeno, S. Farner, *et al*., Physica C **282**, 1413 (1997).

21 Y. Maeno, S. Nishizaki, and Z. Q. Mao, Journal of Superconductivity **12**, 535 (1999).

22 T. M. Riseman, P. G. Kealey, E. M. Forgan, *et al*., Nature **396**, 242 (1998).

23 A. C. Mota, E. Dumont, A. Amann, *et al*., Physica B **259**, 934 (1999).

24 A. Amann, A. C. Mota, M. B. Maple, *et al*., Physical Review B **57**, 3640 (1998).

25 K. Machida, M.-a. Ozaki, and T. Ohmi, Journal of the Physical Society of Japan **65**, 3720 (1996).

26 M. Sigrist and E. Zhitomirsky Michael, Journal of the Physical Society of Japan **65**, 3452 (1996).

27 D. F. Agterberg, T. M. Rice, and M. Sigrist, Physical Review Letters **78**, 3374 (1997).

28 M. Sigrist, D. F. Agterberg, A. Furusaki, *et al*., Preprint , 0 (1999).

29 G. Binnig, A. Baratoff, H. E. Hoenig, *et al*., Physical Review Letters **45**, 1352 (1980).

30 K. Miyake and O. Narikiyo, Physical Review Letters **83**, 1423 (1999).

5 Penetration Depth of Strontium Ruthenate

The results of our measurements of $\lambda(T)$ for Sr_2RuO_4 (SRO) can be summarized very succinctly. We find that SRO has power law behavior in $\lambda(T)$ at low temperatures, specifically $\lambda(T) \propto T^2$ for clean samples. We have observed no sign of a second superconducting phase transition at temperatures down to 40 mK, nor have we seen evidence for a crossover in behavior which might indicate the presence of two independent energy gaps. For a dirty sample, we find that the behavior is similar, but with $\lambda(T) \propto T^3$.

5.1 Samples

Samples for this experiment were provided by the research group of Y. Maeno from Dept. of Physics, Kyoto University, Kyoto, Japan. Crystal growth is described in Ch. 4. Several different samples were provided and these are summarized in Table 1. The critical temperatures of the samples were determined in Japan from measurements of the ac susceptibility. The T_c is taken at the peak of the quadrature component, χ''. The T_c of sample #3 was measured before it was annealed, and not after. From our measurements, it seems that its T_c did not change significantly as a result of annealing.

Table 5.1

Summary of samples

Sample	Crystal	Annealing	Shaped	T_c (K)
#1	C114A2#5	Not annealed	razor blade	1.39
#2	C114A2#3	Not annealed	sandpaper	1.39
#3	C82A1-2a	1500 °C in air for 60 hrs.	razor blade	1.44
#4	C66C2a-1	1050 °C in oxygen for 3 weeks	razor blade	0.82

All samples were cut from larger pieces to a size small enough to fit on the end of our cold finger, approximately 1 mm in diameter. Samples #1, 3 and 4 were shaped by cutting with a razor blade under a microscope. Their perimeter is somewhat irregular as a result of this process, but they are all shaped like flat plates. Sample #2 was cut from the same large crystal as sample #1, but instead of a razor blade, I used fine sandpaper to form the shape. I glued the sample to a glass slide with super glue, leaving a small portion projecting over the edge. By holding the slide vertically I carefully ground the projecting portion of the crystal on 400 grit silicon carbide sandpaper until it was flush with the edge of the slide. The glue was easily dissolved with acetone and the process repeated to form the remaining edges of the sample. In this way I prepared the sample in a fairly regular octagonal shape.

5.2 Calibration

We tried both of the calibration techniques discussed in Ch. 1. We found that the aluminum sphere technique overestimates the change in penetration depth. For the second calibration procedure I fashioned a dummy sample of high purity aluminum (sample Al#1) in the same shape and size as sample #3. This technique worked more successfully. In Fig. 5.1 the data for the Al#1 sample are compared with the theoretical curve of $\lambda(0)^2/\lambda(T)^2$. I have taken the values for pure aluminum as $\lambda(0) = 500$ Å and $\Delta(0) = 0.18$ meV. As discussed in Ch. 2, I used the weak coupling interpolation formula for $\Delta(T)$ and the expression for $\lambda(T)$ appropriate for a non-local superconductor. The value of T_c which best fits the data is 1.16 K, which compares favorably with the value of 1.18 K from tables. I found that by adjusting the geometrical scaling factor to a value of $G = 2.5$ Å/Hz for the Al#1 sample, the data could be made to lie directly over the theoretical curve. Since G depends only on the geometry of the sample and coil, this same value can be used to scale the data for sample #3. We discovered only relatively

late in the course of this study that the first calibration procedure was not adequate. Rather than make a dummy sample for every SRO sample, I have used the results of the sample #3 calibration. By comparing the data from other samples with the calibrated data from sample #3 we can estimate the geometry factor for the other samples.

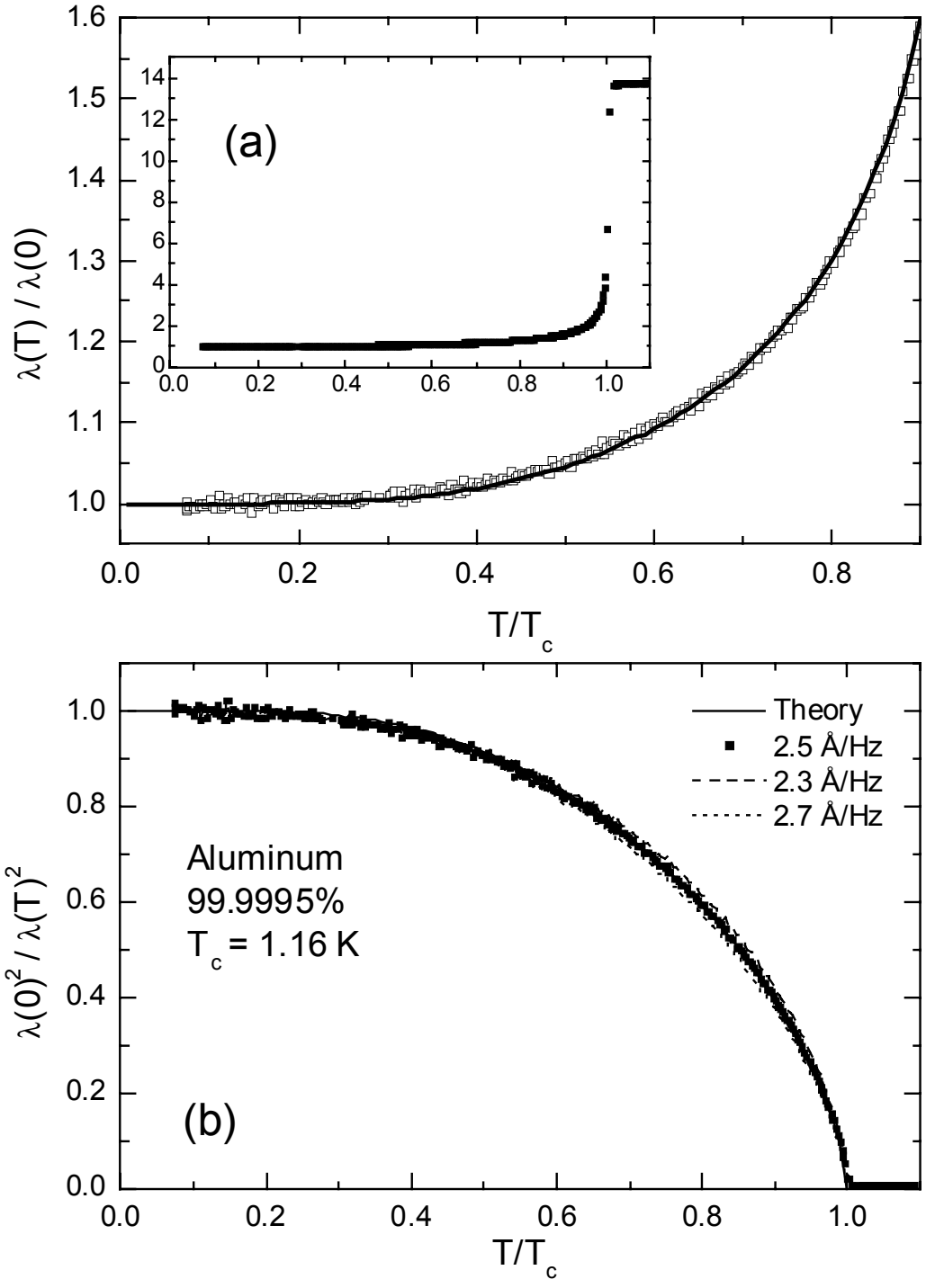

Figure 5.1

Comparison of $\lambda(T)$ with theory for sample Al#1, 99.9995% aluminum. (a) Inset shows the full temperature range. Main graph shows low temperature detail. (b) Plot of the superfluid fraction. The scaling factor which best fits the theory is $G = 2.5$ Å/Hz.

5.3 Results

Results for the high purity aluminum sample, Al#1, are shown in Fig. 5.1. Graph (a) shows $\lambda(T)$ plotted as a function of T/T_c. Graph (b) shows $\lambda(0)^2/\lambda(T)^2$ as a function of T/T_c, which is proportional to the superfluid density. The agreement with the theoretical curve is excellent, when the scale factor G = 2.5 Å/Hz. To give an idea of the sensitivity of the shape of the curve to the value of G, the dashed lines show the dependence of the data when G is varied ±10%. Because sample Al#1 was prepared with nominally the same shape as SRO sample #3, we use this value of G, adjusted slightly to account for the very small difference in shape, to scale the data for sample #3. Likewise, the various shapes of each of the other samples were used to determine values of G relative to sample #3. Figure 5.2 summarizes the penetration depth for samples #1-4 with the magnetic field oriented perpendicular to the *ab*-planes of the crystals. On this scale, the general behavior of all four samples is quite similar, but there are clear differences in the location and sharpness of the transitions. Sample #3 has the highest T_c = 1.44 K, and also shows the sharpest transition. It is interesting to note the difference between samples #1 and 2, which are cut from the same crystal. Sample #2 shows a much more rounded transition as a result of the damage that occurred on the surface as a result of grinding it on sandpaper. Sample #3 has a significantly lower T_c = 0.82 K.

Figure 5.3 shows the temperature region from T/T_c = 0 to 0.8, plotted against $(T/T_c)^2$ for samples #1-3. It is evident from these graphs that at temperatures below approximately 0.4 T_c, all three samples have $\Delta\lambda(T) \propto T^2$. In addition, a graph of sample #3 is shown with the field oriented parallel to the *ab*-planes. The temperature dependence is virtually identical to the perpendicular orientation, showing quadratic temperature dependence below 0.4 T_c. Figure 5.4 shows a detail of the low temperature region, below 0.7 K, for sample #2 as a function of T^2.

The clear linear behavior displayed indicates once again that $\Delta\lambda(T) \propto T^2$ at low temperature and is typical of samples #1-3.

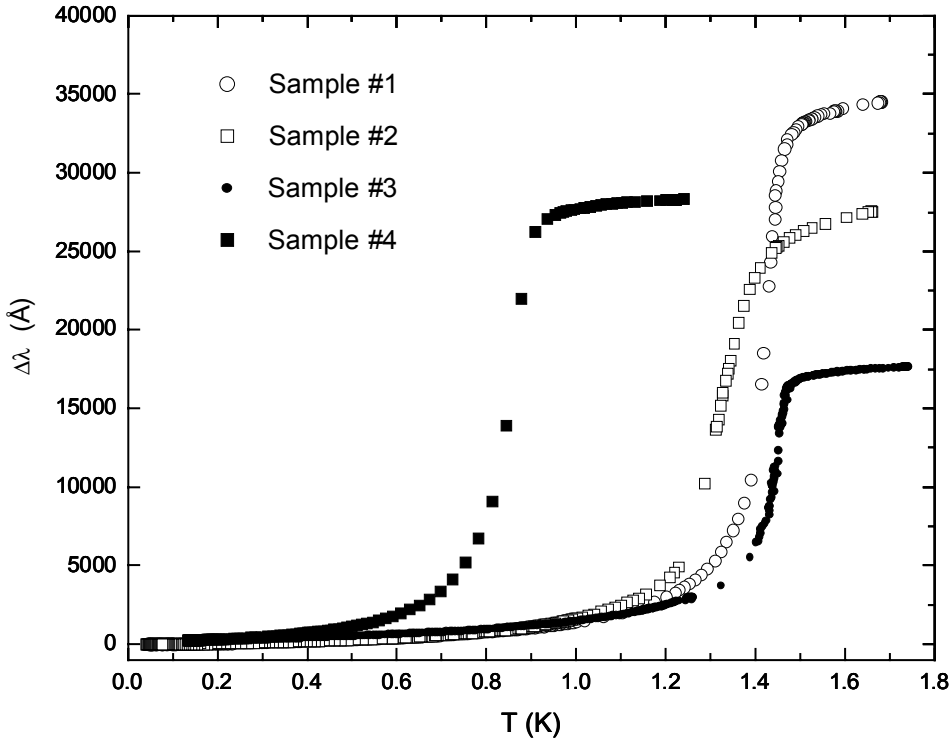

Figure 5.2

Penetration depth of SRO samples #1-4 with magnetic field oriented perpendicular to the *ab*-planes of the crystals.

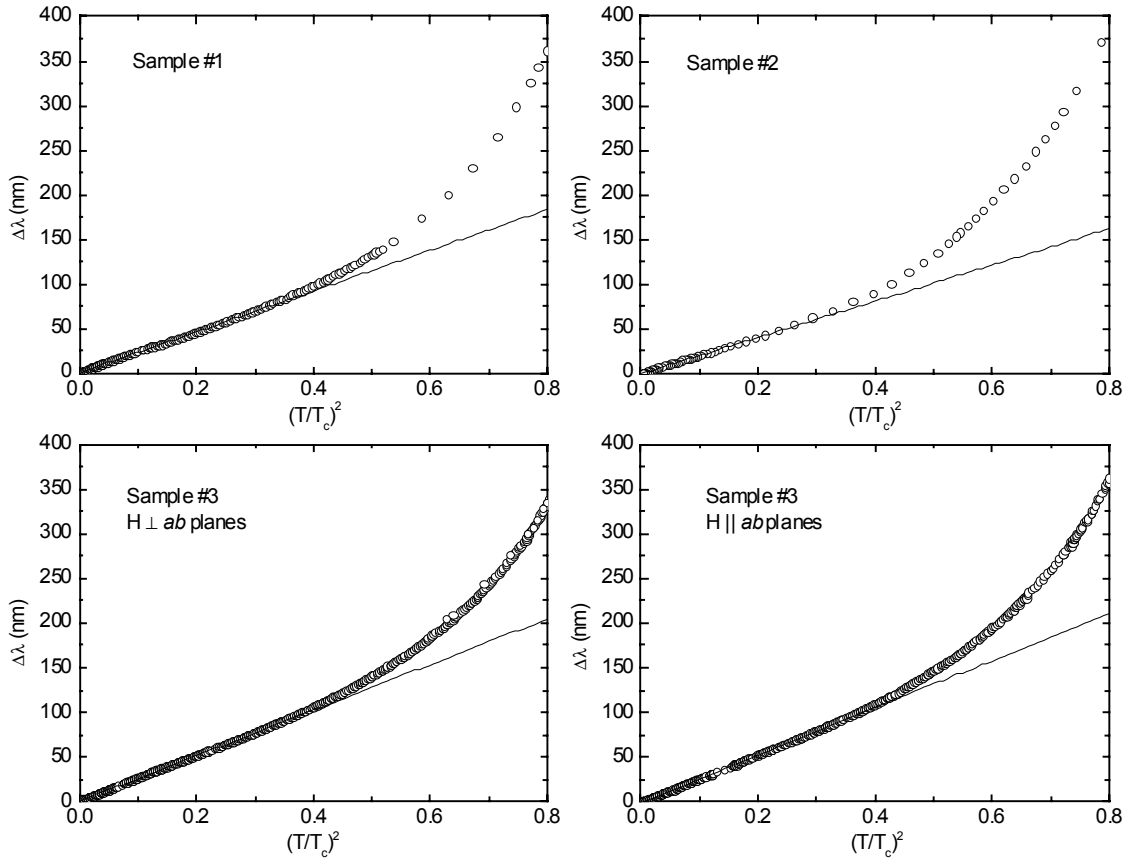

Figure 5.3

Temperature dependence of penetration depth for samples #1-3. All samples are measured with magnetic field oriented perpendicular to the *ab*-planes of the crystals. Sample #3 is also shown with magnetic field parallel to the *ab*-planes. Note that the scales are identical on all four graphs.

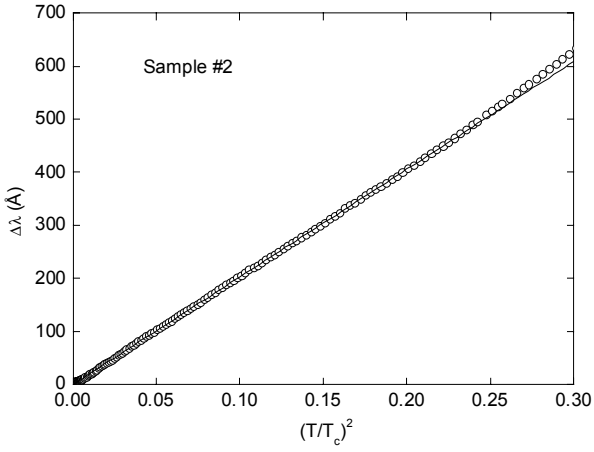

Figure 5.4

Penetration depth of sample #2 (T_c = 1.39 K) at low temperatures, plotted as a function of $(T/T_c)^2$. It is clear from this behavior that $\lambda(T) \propto T^2$ at low temperatures.

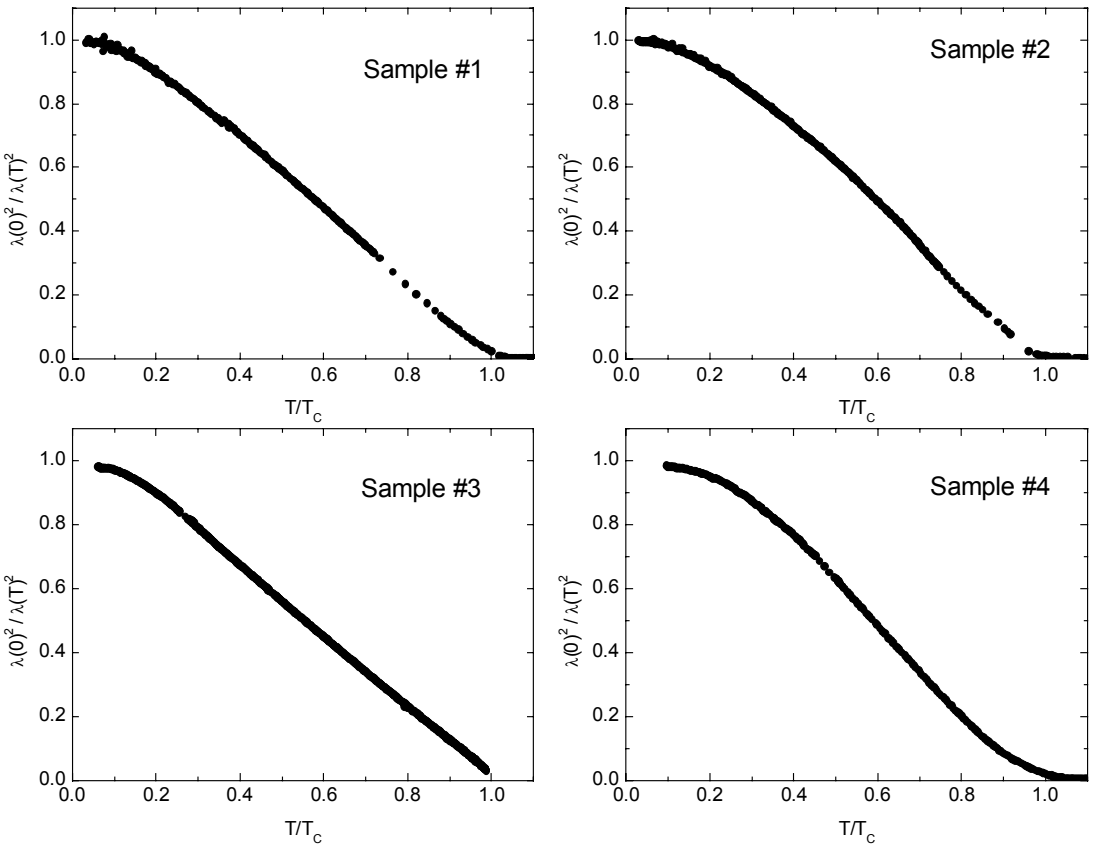

Figure 5.5

Summary of temperature dependence of $\lambda(0)^2 / \lambda(T)^2 \propto n_s(T)/n_s(0)$, the superfluid fraction, for samples #1-4. The value of $\lambda(0)$ = 1900 Å is used for samples #1-3, and $\lambda(0)$ = 2230 Å is used for sample #4.

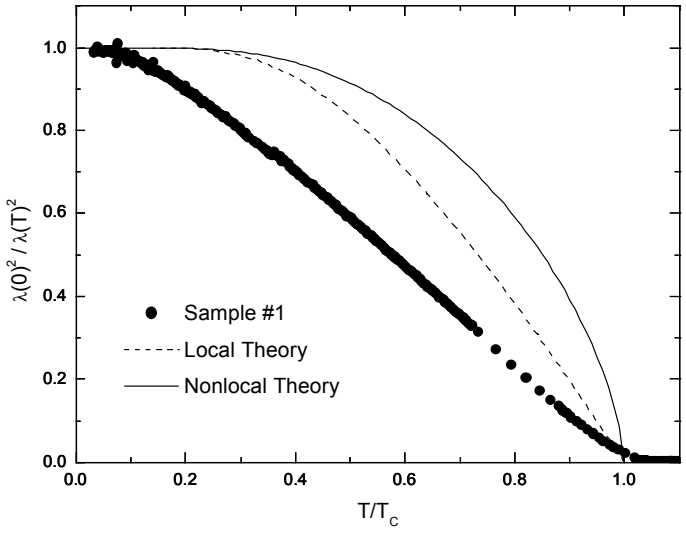

Figure 5.6

Comparison of superfluid fraction of sample #1 with local and nonlocal *s*-wave models.

5.4 Interpretation

Our observation of power law behavior implies that the energy gap has nodes. The non-unitary and orbital dependent superconductivity (ODS) models of superconductivity are inconsistent with this result. As discussed in the previous chapter, there are several possible scenarios under the ODS model. The simplest is an energy gap on one Fermi surface sheet, and none on the other. This would give exponential dependence of $\lambda(T)$, contrary to our observation of power law dependence. We see evidence neither for a second superconducting transition nor for the crossover of temperature dependence which might result from two different energy gaps. Likewise, the non-unitary model predicts an exponential dependence with does not appear in SRO.

Our observation of temperature dependence of $\Delta\lambda(T) \propto T^2$ can be taken as strong evidence that the energy gap has nodes, as discussed in Ch. 3. The naïve conclusion might be that the T^2 dependence implies that there are point nodes. However, it has been found experimentally that low temperature NMR spin relaxation rate $1/T_1 \propto T^3$,[1] and electronic specific heat $C_e \propto T^2$.[2] Both of these (in my opinion, highly credible) results are consistent with *line* nodes in the gap. Therefore, we need to consider carefully whether our results are consistent with these and other measurements made up to now on SRO. In the local limit, in the absence of impurities, the penetration depth will show *linear* temperature dependence in the presence of line nodes. We are faced with the same dilemma which confronted those studying the cuprates, when early measurements of $\lambda(T)$ showed quadratic behavior. Thanks to the work on the cuprates there are a number of well documented possibilities to explore. We believe that our data are consistent with line nodes in the energy gap when we take into account one or more of these effects.

5.4.1 Resonant Impurity Scattering

As discussed in Ch. 3, Hirschfeld and Goldenfeld[3] noted that the effect of resonant impurity scattering (RIS) on the cuprate superconductors is to change the intrinsic $\lambda(T) \propto T$ to quadratic, and this would be the most obvious explanation for quadratic dependence in SRO. It is possible that just such an effect is at play in our measurements of SRO. Hirschfeld and Goldenfeld introduce a crossover temperature T^*, below which the intrinsic linear behavior due to line nodes would be modified by RIS to quadratic. For the strong scattering limit, the T_c suppression (T_{c0} - T_c)/T_{c0} is estimated to be on the order of Γ/Δ_0, where T_{c0} is the critical temperature in the absence of impurities, Γ is the scattering rate, and Δ_0 is the maximum energy gap. For very small impurity levels the crossover temperature will be approximately $T^* \sim (\Gamma\Delta_0)^{1/2}$. So we can estimate that $T^* \sim \Delta_0\left(\frac{T_{c0}-T_c}{T_{c0}}\right)^{1/2}$. Taking $\Delta_0 = 1.76\ T_c$, and T_{c0} = 1.5 K, we find $T^* \sim 0.7$ K. This value is close to the range over which the T^2 dependence was found to fit the data for samples #1-3. However, we do not observe a linear dependence in any temperature range in any of the samples we have measured. It could be that the value of T^* is so high that linear behavior, which would only show up in the low temperature limit, is hidden by the nonlinearity that normally appears at higher temperatures. For example in the best measurements of the cuprates, linear temperature dependence is observed at temperatures below around 15-25% of T_c. In our measurements, since T^* and the range of quadratic behavior is about half of T_c, it is possible that the linear range is simply not observable. Were they available to us, it is conceivable that measurements on even cleaner samples might exhibit a clear crossover between quadratic and linear behavior.

While cleaner samples were not immediately available, dirty samples are plentiful. To attempt to clarify the role of impurity scattering, we measured $\Delta\lambda(T)$ for sample #4 with T_c = 0.82 K, significantly lower than the optimal value of 1.5 K. The suppression of T_c is presumed to be due to the presence of disorder, either in the form of lattice defects, non-magnetic impurities, or both. Our results are shown in Fig. 5.7. In contrast to the clean samples, where quadratic dependence is observed, we find that the dirty sample shows $\Delta\lambda(T) \propto T^3$ at low temperatures.

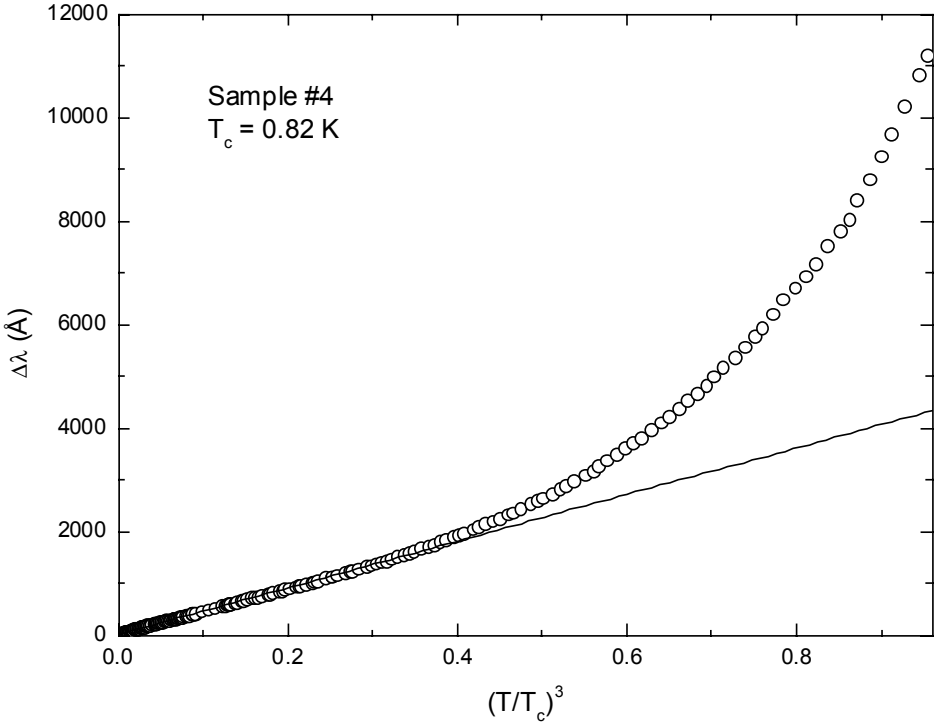

Figure 5.7

Penetration depth of sample #4 as a function of $(T/T_c)^3$. The greater level of impurities and /or defects in this sample cause the cubic dependence, rather than the quadratic dependence observed in clean samples.

5.4.2 Nonlocal Effects

We might be able to understand this result by considering the scenario of nonlocal effects proposed by Kosztin and Leggett,[4] also discussed in Ch. 3. They calculate, for an unconventional superconductor with nodes in the energy gap, that nonlocal effects may be important in regions of *k*-space close to the nodes. If the magnetic field is oriented parallel to the *c*-axis of a cuprate crystal, with the field penetrating into the *a* or *b* direction, this will give quadratic behavior below a crossover temperature $T^* = \xi_0 \Delta_0 / \lambda_0$, where ξ_0 and λ_0 are the superconducting coherence length and penetration depth at zero temperature, respectively. Let us examine this possibility for SRO. From the literature we find $\xi_0 \sim 660$ Å and $\lambda_0 \sim$ 1800-1900 Å.[2, 5, 6] Estimating the energy gap by the weak coupling value 1.76 $T_c \sim 2.6$ K, gives us an estimate of $T^* \sim 0.95$ K. This value is nearly as large as T_c. According to this criterion, assuming that SRO has nodes, we could expect that instead of a crossover to nonlocal behavior, as suggested for the cuprates, SRO could behave nonlocally over almost its entire temperature range! Some estimates of the energy gap from point contact spectra[7] show an anomalously high value, $\Delta_0 \sim 13$ K, which would raise our estimate of T^* well above T_c.

Kosztin and Leggett propose a simple test for this nonlocal behavior. For the cuprates, if the orientation of the magnetic field relative to the sample is modified such that the field is parallel to the *ab* planes, with field penetrating in the *c* direction, then no nonlocal effects should be observed. This result assumes the material is quasi-two-dimensional, dominated by *k* vectors within the planes. In this orientation, *k*-space directions where the Fermi surface and OP are nonvanishing (in the *ab* planes) are parallel to the surface. SRO is considered to be quasi-two-dimensional. The ratio of the coherence lengths parallel and perpendicular to the

planes[2] is $\xi_{ab}/\xi_c = 20$, which is quite large (although the cuprates have values closer to 100). I believe that if we assume the presence of nodes then the model should apply equally to SRO.

We measured $\lambda(T)$ for sample #3 with the field oriented parallel to the planes. This was accomplished by attaching a small plastic cube to the end of the cold finger, and gluing the crystal against the side of the cube, with its edge contacting the end of the cold finger. However, our measurements give the same result for this field orientation: $\lambda(T) \propto T^2$, in seeming conflict with the nonlocal theory. However, because the cube was fashioned by hand, I estimate that the orientation is only parallel to within ~5-10°. It is possible that the small misorientation is sufficient to allow a component of the screening currents flowing in the direction where the nonlocal effect appears. To rule this out one could attempt a more careful orientation of the sample and field. But the effect might be so sensitive to orientation that it would be necessary to construct a system which would allow in-situ adjustment of the angle. An additional effect could come from the *c*-axis penetration depth which participates in the effect when the field is oriented in this direction. It is possible that the temperature dependence of λ_c could dominate, obscuring the intrinsic dependence of the in-plane penetration depth in this orientation.

Another explanation for the cubic behavior in the dirty sample is more interesting. Kosztin and Leggett find, more generally, that if the intrinsic behavior in the local limit is $\Delta\lambda(T)$ then taking into account nonlocal effects, we would expect $\Delta\lambda_{nonlocal}(T) \propto T \cdot \Delta\lambda(T)$. Let us assume that the clean samples have intrinsic linear behavior in the absence of the nonlocal effect. Then we would expect quadratic behavior when we take into account the nonlocal effect. Similarly, let us assume that the dirty sample, due to impurity scattering, would have

quadratic behavior in the absence of nonlocal effects. Then we might expect to observe cubic dependence in this sample when the nonlocal effect is included.

In general, the effect of impurities on a nonlocal superconductor is to drive it towards more local behavior with increasing impurity content, because the coherence length is reduced and the penetration depth is increased. We need to estimate to what extent the dirty sample can still be considered nonlocal. Mackenzie *et al*.[8] studied systematically the dependence of T_c on non-magnetic impurities in SRO. Using their estimates for mean free path, interpolated from their graph of resistivity $\rho(T)$, I estimate that sample #4 has a mean free path $\ell \sim 1750$ Å. This value, while significantly suppressed from the clean sample value of ~7000 Å, is still larger than the clean sample coherence length of $\xi_0 = 660$ Å. Impurities can be expected to reduce the coherence length to a value[9]

$$\frac{1}{\xi} = \frac{1}{\xi_0} + \frac{1}{\ell}. \tag{5.1}$$

Putting in the values I find $\xi \sim 480$ Å. We can also estimate the effect of impurities on the effective zero-temperature penetration depth, which should be greater in a dirty sample because scattering from impurities reduces the superfluid density, thereby reducing the screening of the magnetic field. The effective penetration depth can be expressed as

$$\lambda_{eff}(\ell, T) = \lambda(T)\left(\frac{\xi_0}{\xi}\right)^{1/2}. \tag{5.2}$$

I estimate $\lambda_{eff}(T=0) = 2230$ Å. Using ξ and $\lambda_{eff}(0)$, and assuming that the gap, Δ_0, is not strongly affected by impurities, I estimate $T^* = \Delta_0 \xi / \lambda = 0.6$ K. This value is identical to the range over which we can fit cubic dependence in sample #4. The precise agreement is somewhat coincidental, considering the crude approximations used in this estimate. However, it

is suggestive that this model combining nonlocality and impurity scattering might apply in the case of SRO and, if correct, would support the conclusion that the clean samples have line nodes in the gap. One might further test this conclusion by measuring a sample with critical temperature in the intermediate range between the samples measured here, say 1.2 K.

5.4.3 High Frequency Effects

Historically, in the heavy fermion superconductors, there was an inconsistency in measurements of $\lambda(T)$ at low temperatures. These unconventional superconductors are believed to have line nodes in the energy gap as well. These materials are exquisitely sensitive to impurities and defects, and resonant impurity scattering was considered important, as in the cuprates. However, an additional effect was noted by Signore *et al*.,[10, 11] who found that the response of very clean samples of UPt_3 ($T_c \sim 0.5$ K) was dependent upon the frequency of measurement. Signore *et al*. showed that for low frequencies (from DC to at least 5 kHz) the temperature dependence $\lambda(T) \propto T$, while at frequencies above 3 MHz, $\lambda(T) \propto T^2$. The effect of frequency can generally be ignored for ordinary superconductors until the frequency exceeds the energy gap (in the GHz range) where Cooper pairs can be broken by the absorption of photons. However, in an unconventional superconductor with nodes in the energy gap, it is possible for significantly lower frequencies to break Cooper pairs in the region of the nodes. This effect could be manifested in SRO in our experiments because our measurement frequency is tens of MHz. The only way to rule out this effect would be to construct an entirely new apparatus, such as a SQUID or mutual inductance system, to measure the penetration depth at lower frequency.

References

1 K. Ishida, (Private communication, 1999).

2 Y. Maeno, S. Nishizaki, and Z. Q. Mao, Journal of Superconductivity **12**, 535 (1999).

3 P. Hirschfeld, J. and N. Goldenfeld, Physical Review B **48**, 4219 (1993).

4 I. Kosztin and A. Leggett, Physical Review Letters **79**, 135 (1997).

5 T. M. Riseman, P. G. Kealey, E. M. Forgan, *et al*., Nature **396**, 242 (1998).

6 C. M. Aegerter, S. H. Lloyd, C. Ager, *et al*., Journal of Physics: Condensed matter **10**, 7445 (1998).

7 F. Laube, G. Goll, H. v. Lohneysen, *et al*., **cond-mat/9907267** (1999).

8 A. P. Mackenzie, R. K. W. Haselwimmer, A. W. Tyler, *et al*., Physical Review Letters **80**, 161 (1998).

9 M. Tinkham, *Introduction to Superconductivity* (McGraw-Hill, Inc., New York, 1996).

10 P. J. C. Signore, B. Andraka, M. W. Meisel, *et al*., Physical Review B **52**, 4446 (1995).

11 P. J. C. Signore, J. P. Koster, E. A. Knetsch, *et al*., Physical Review B **45**, 10151 (1992).

6 Conclusions and Future Directions

I have shown that the temperature dependence of the penetration depth is a valuable measurement technique for probing the behavior of the order parameter in unconventional superconductors. We have constructed a high resolution tunnel-diode oscillator-based measurement system suitable for measuring the temperature dependence of the magnetic penetration depth of superconductors, $\lambda(T)$, at very low temperatures. I have reported on measurements of $\lambda(T)$ in high quality single crystals of the unconventional perovskite superconductor Sr_2RuO_4 (SRO) down to 0.04 K. We observe quadratic temperature dependence at low temperatures. I have argued that power law behavior is consistent with an energy gap with nodes. We believe that SRO has line nodes, and propose several possible mechanisms to explain the observed quadratic dependence. We propose that non-local effects may be more important in determining the temperature dependence than impurity scattering, and is sufficient to explain the deviation from the linear behavior expected for local superconductors with line nodes.

Our results appear to be inconsistent with the leading theories of superconductivity in SRO. Both the orbital dependent superconductivity (ODS) model and the non-unitary model predict exponential temperature dependence at low temperatures, because the magnitude of the energy gap is isotropic. In addition, there is no sign of the crossover or second phase transition predicted by the orbital dependent superconductivity model.

In a December 1998 article in *Nature*,[1] Maurice Rice described the ODS model as "a complete description of the unconventional superconductivity of Sr_2RuO_4," and declared that the consensus understanding of SRO as a two-dimensional analog of the A-phase of superfluid ^{3}He was, at that time, well established. Our measurements have shown that what once seemed

clear is again muddy. SRO displays some of the features of the ODS model (triplet spin symmetry, time reversal symmetry breaking) but the low temperature penetration depth fails to agree with the theory. It is time to reevaluate the picture of SRO, especially in relation to other unconventional superconductors.

SRO combines the properties of a number of unconventional superconductors. Our measurements show that, in addition to the perovskite crystal structure, SRO shares with the cuprates a gap structure with line nodes of some sort. In common with the heavy fermion superconductors and superfluid ^{3}He-A, SRO displays triplet pairing and time reversal symmetry breaking. If we add to this picture the likely scenario that SRO is, in fact, a nonlocal superconductor, we must then begin to understand a material that is in some ways familiar and in other ways rather unfamiliar.

6.1 Future Directions

There are several experiments which could be performed in the future which might help clarify our understanding of SRO. While our measurements were made on samples of the highest quality available today, measurements of the penetration depth in the future on crystals of even higher quality may prove valuable in elucidating the role of impurities and defects. As in the measurements of the cuprates, we may find that a more consistent picture emerges when further control is gained over impurity and defect levels in these samples. In addition, it might prove fruitful in understanding the role of defects and impurities to extend the measurements reported here on a crystal of intentionally lower quality, by measuring samples with a range of different critical temperatures. In Ch. 1 I discussed a number of different techniques for measuring the penetration depth. While the self-inductive tunnel-diode oscillator technique which we employed is one of the best ways of making precision measurements of temperature

dependence, it would be gratifying to see some of the other techniques employed for comparison. In particular, those techniques which operate at lower frequency, such as mutual inductance and SQUID measurements, would be useful in eliminating the possibility of pair-breaking effects at high frequency. The addition of a small Helmholtz coil to our oscillator system would allow us to apply a magnetic field to the sample and possibly observe the time reversal symmetry breaking effects reported by Mota *et al*.[2]

One of the best ways of unambiguously determining the symmetry of the order parameter is to employ a method sensitive to the phase rather than the amplitude. Such an experiment was performed on the cuprate YBCO by Wollman *et al*.[3] in our research group using Josephson tunneling from a conventional *s*-wave superconductor into YBCO in a SQUID geometry which creates interference between different directions in *k*-space. A member of our group is attempting to make similar measurements on SRO using indium contacts on SRO crystals.

6.1.1 Other Materials

As discussed in previous chapters, the penetration depth in the cuprates has a linear temperature dependence at temperatures down to approximately 1 K. There are a number of interesting determinations that remain to be made below 1 K in these materials. For example, both the resonant impurity scattering and nonlocal models predict that the penetration will cross over from linear to quadratic temperature dependence at very low temperatures. The crossover from linear to quadratic dependence was explored systematically by Bonn *et al*.[4] as part of a study of the effect of the introduction of Zn and Ni impurities into YBCO. In this case the crossover temperature, T^*, from linear to quadratic dependence is increased by addition of impurities. But it would be interesting to attempt to observe T* in a pure sample by going to very low temperatures. Another potentially important result concerns an observation, made by

Movshovich *et al*., of an anomaly in the thermal conductivity of BSCCO doped with Ni as a magnetic impurity. They report a dramatic drop in thermal conductivity at ~0.2 K which they interpret as the opening of a full energy gap in the region of the nodes as a result of a second phase transition. One of our first goals when this project began was to attempt measurements of these effects, and we focused on these in the early stages. However, we found that several factors precluded good measurements. The signal to noise ratio depends on the intrinsic change in the penetration depth which occurs, and also on the filling factor of the sample within the measurement coil. Both of these factors were working against us in the cuprate measurement, as the intrinsic change in penetration depth is very small at these temperatures, and the samples to which we had access were also very small. However, armed with this knowledge, it should be possible to obtain larger samples of doped cuprates and may be possible to construct a system which would be able to detect this very small effect in the penetration depth.

The opportunity exists to measure a number of other materials using our system. For example, recently a family of borocarbide superconductors was discovered with the formula RNi_2B_2C, where R stands for one of the rare earth elements Y (Yttrium), Lu (lutetium), Tm (thulium), Er (erbium), Ho (holmium), or Dy (dysprosium). (See Canfield *et al*.[5] for a recent review.) One of the remarkable properties of these materials is the coexistence of antiferromagnetic and superconducting order. Because the rare earth elements have closely similar chemical properties, and because the magnetic moments of their nuclei vary in a consistent way across the periodic table, the interaction between magnetic and superconducting properties can be studied systematically. We have begun to make some measurements of the temperature dependence of the penetration depth in these materials. Shown in Fig 6.8 are preliminary results for the nonmagnetic member of the family, $LuNi_2B_2C$.

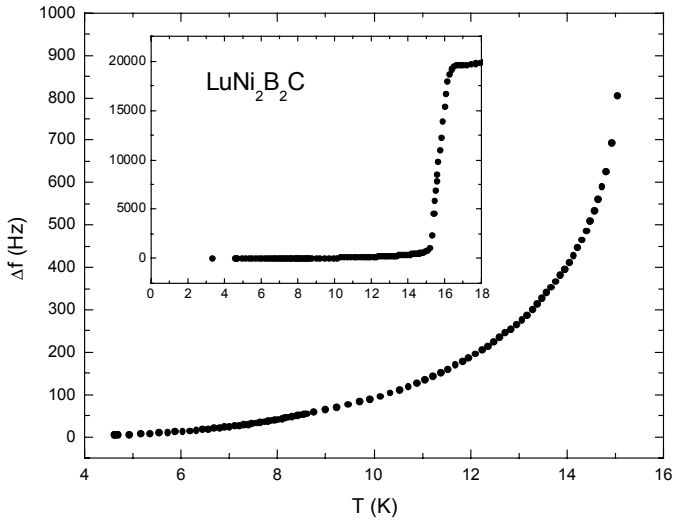

Figure 6.8
Preliminary, uncalibrated results for $\lambda(T)$ for $LuNi_2B_2C$. The inset shows the full temperature range.

From this and subsequent measurements, it appears that $LuNi_2B_2C$ may be a conventional *s*-wave superconductor. Some of the early measurements on one of the magnetic members of the family, $HoNi_2B_2C$, shows a richly detailed structure, with reproducible jumps in the susceptibility at a number of different temperatures. University of Illinois graduate student Elbert Chia will be continuing these studies as part of his thesis research.

References

1 M. Rice, Nature **396**, 627 (1998).

2 A. C. Mota, E. Dumont, A. Amann, *et al*., Physica B **259**, 934 (1999).

3 D. A. Wollman, D. J. Van Harlingen, J. Giapintzakis, *et al*., Physical Review Letters **74**, 797 (1995).

4 D. A. Bonn, S. Kamal, K. Zhang, *et al*., Physical Review B **50**, 4051 (1994).

5 P. C. Canfield, P. L. Gammel, and D. J. Bishop, Physics Today **51**, 40 (1998).

Appendix A Samples

This appendix contains a series of photographs and lists of pertinent data on each of the samples discussed in this thesis.

A.1 Crystal Batches

The SRO crystals were grown by Y. Maeno, Dept. of Physics, Kyoto University, Kyoto, Japan. A graph of the ac magnetic susceptibility was provided for a representative sample from the same batch as each of the samples we were given. This serves as an accurate measure of the critical temperature, and the sharpness of the transition is indicative of the quality of the samples. The graphs are reproduced here. The top graph in each figure is the real part of the complex susceptibility, χ', and the lower graph is imaginary part, χ''. The critical temperature is determined by the peak in χ''.

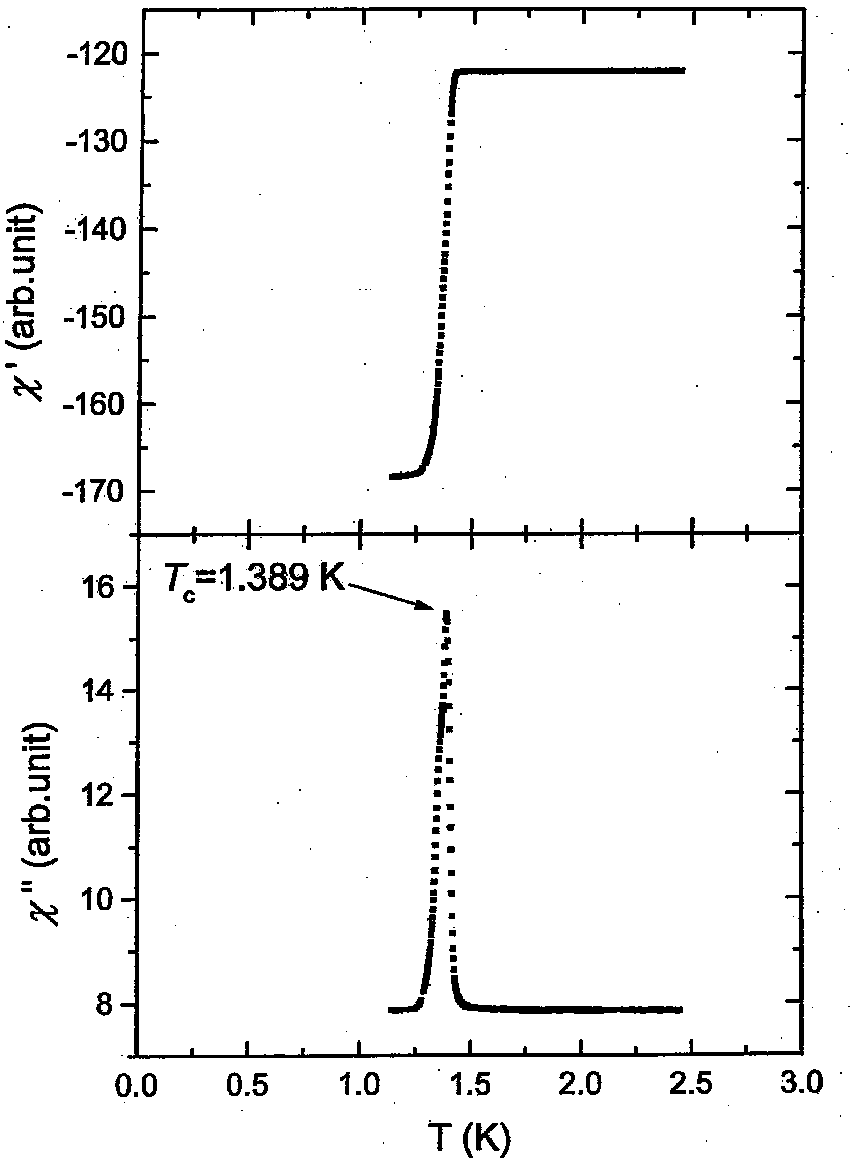

Figure A.1
AC susceptibility of representative crystal from batch C114A (Samples #1 and 2)

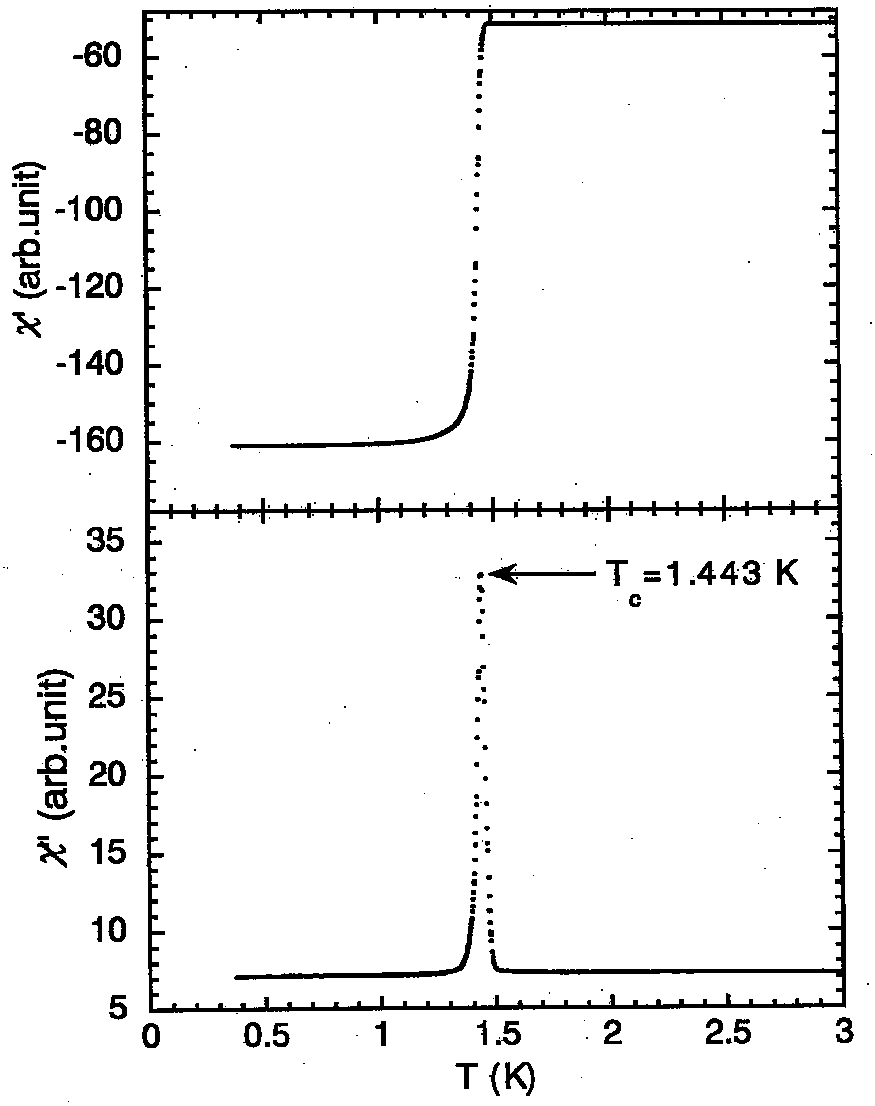

Figure A.2
AC susceptibility of representative crystal from batch C82A1-2a (Sample #3)

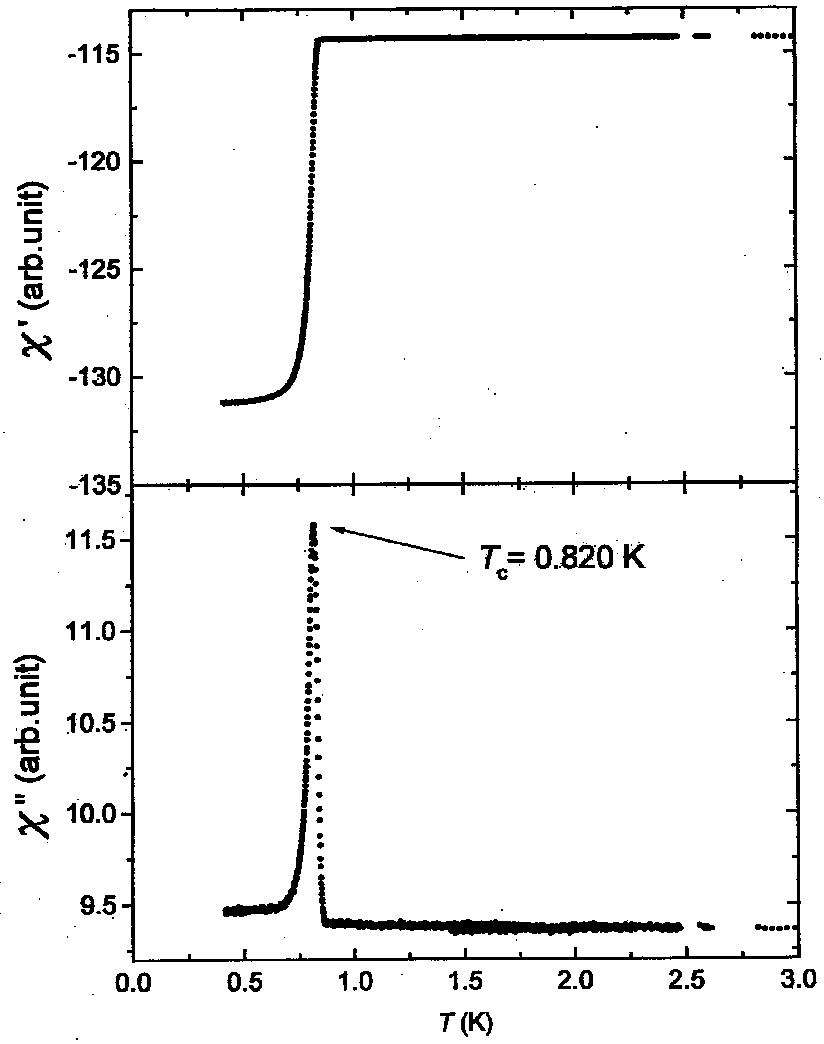

Figure A.3
AC susceptibility of representative crystal from batch C66C2a (Sample#4)

A.2 SRO Sample Geometry

A.2.1 SRO Sample #1

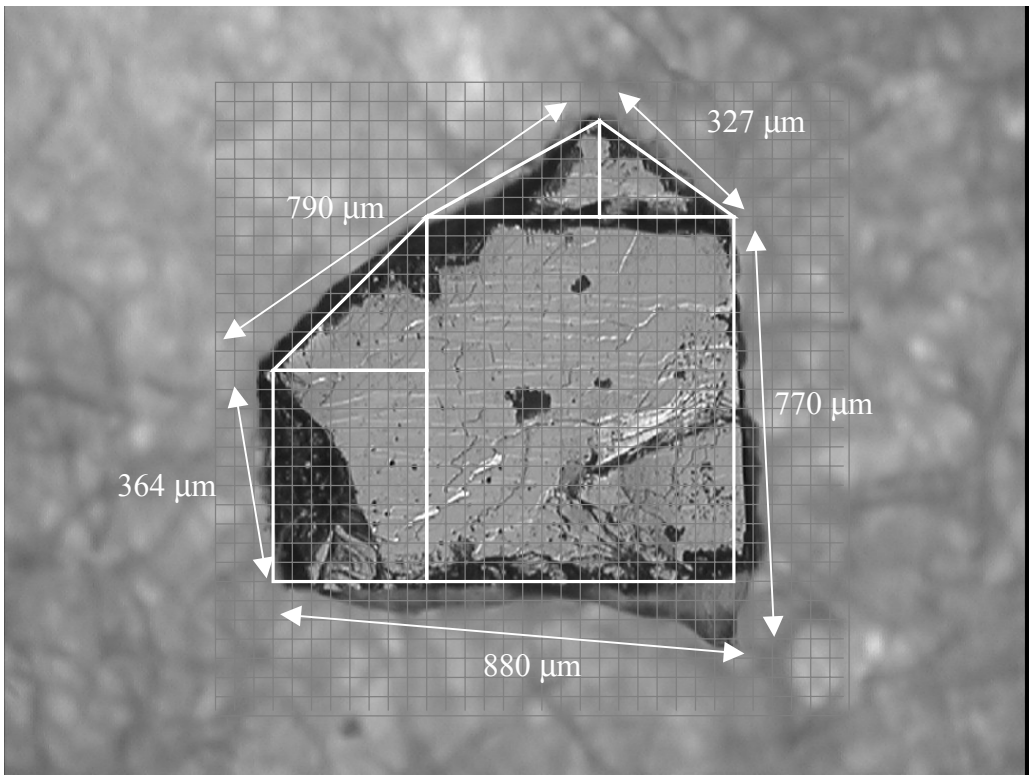

Figure A.4

Sample #1dimensions

Batch		C114A
Critical Temp.	T_c	1.39 K
Thickness	t	130 μm
Total area	A	0.630 mm^2
Perimeter	P	3131 μm
Frequency	f	11.8 MHz
Sphere Shift	Δf_{sphere}	11 kHz

A.2.2 SRO Sample #2

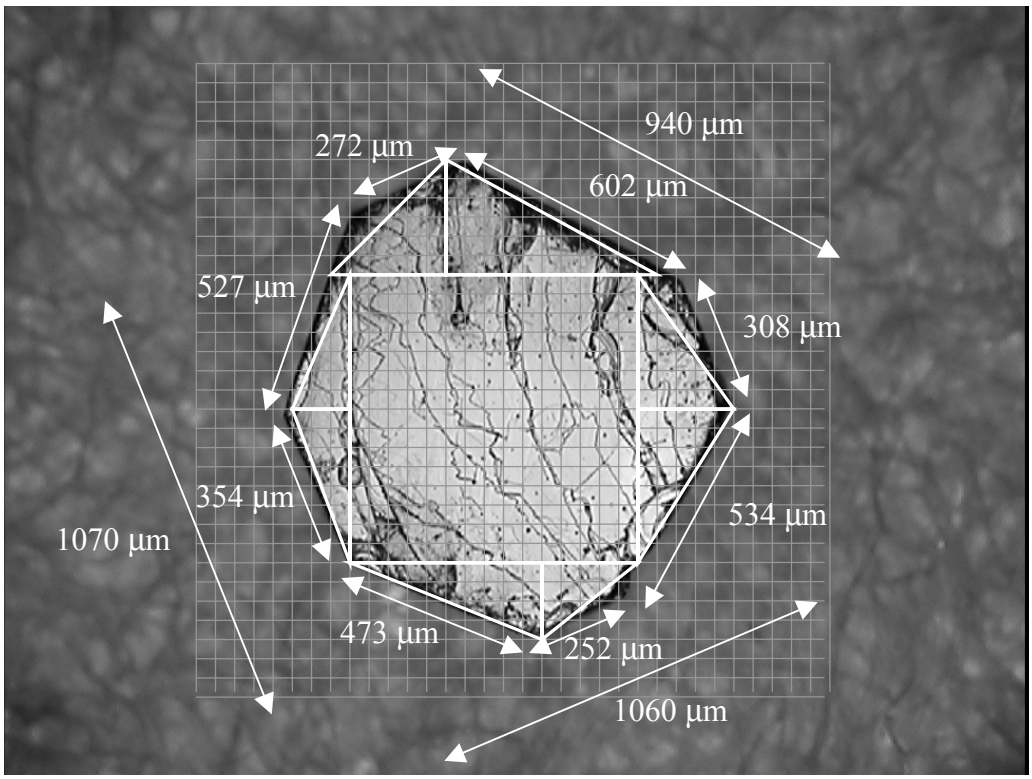

Figure A.5

Sample #2 dimensions

Batch		C114A
Critical Temp.	T_c	1.39 K
Thickness	t	100 µm
Total area	A	0.801 mm^2
Perimeter	P	3322 µm
Frequency	f	17.38 MHz
Sphere Shift	Δf_{sphere}	16 kHz

A.2.3 SRO Sample #3

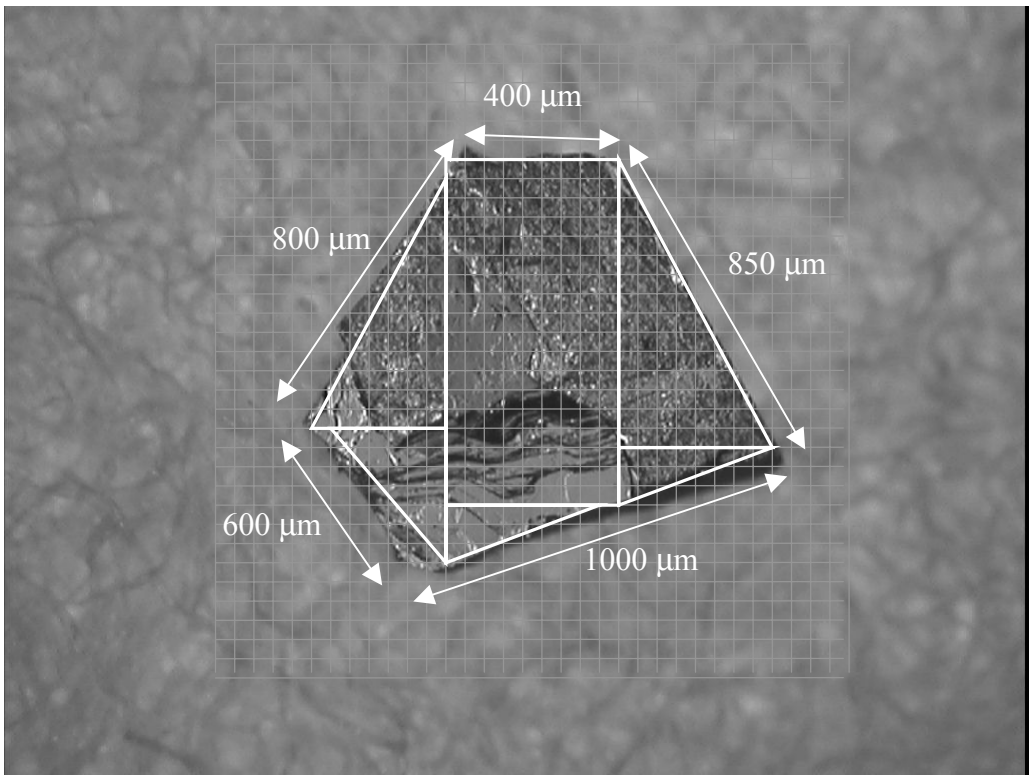

Figure A.6

Sample #3 dimensions

Batch		C82A1
Critical Temp.	T_c	1.44 K
Thickness	t	126 μm
Total area	A	0.988 mm^2
Perimeter	P	3650 μm
Frequency	f	28.2 MHz
Sphere Shift	Δf_{sphere}	89 kHz

A.2.4 SRO Sample #4

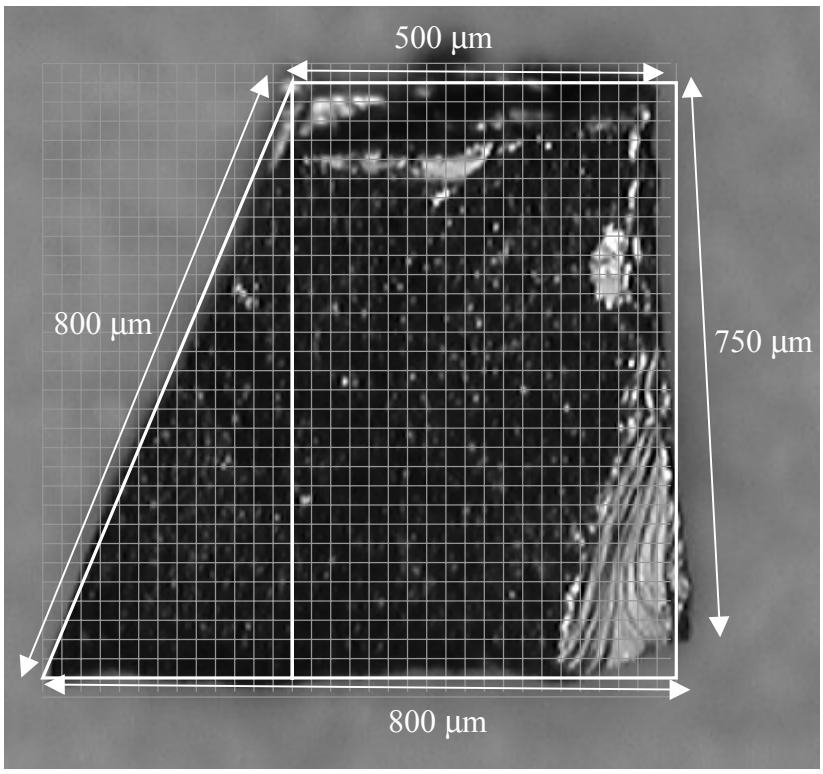

Figure A.7

Sample #4 dimensions

Batch		C66C2a
Critical Temp.	T_c	0.82 K
Thickness	t	250 μm
Total area	A	0.465 mm^2
Perimeter	P	2850 μm
Frequency	f	28.2 MHz
Sphere Shift	Δf_{sphere}	89 kHz

Vita

Brian David Yanoff was born on May 30, 1971, in Philadelphia, Pennsylvania. He attended Swarthmore College where, in addition to majoring in physics with a minor in computer science, he also met his wife, Liz. During the summers of 1991 and 1992 he worked with Swarthmore Professor Peter Collings on light scattering experiments to study the phase transition between the isotropic liquid and the A* liquid crystal phases. Brian was elected a junior member of Sigma Xi, the scientific research society, in 1993. After graduating with honors in 1993, Brian's fascination with phase transitions and the use of computers in condensed matter research led him to the University of Illinois, where, in the summer of 1994, he began work in the research group of Prof. Dale Van Harlingen. His initial projects concerned the behavior of superconductors in mesoscopic systems, but he soon turned to a study of the symmetry of the unconventional heavy fermion superconductor UPt_3, attempting a rather difficult phase sensitive measurement of the order parameter. In November 1998 he began a collaboration with postdoc Ismardo Bonalde, to study the temperature dependence of the magnetic penetration depth in a number of unconventional superconductors at very low temperatures. Following graduation Brian will begin work at the General Electric Company's Corporate Research and Development Center, in Schenectady, NY, to help design and develop digital x-ray detectors for medical applications.